TITLE

Precise generation of bystander-free mouse models with ABE9-SpRY.

AUTHORS

Jun Kai Ong[1,5], Sayari Bhunia[1,2,3], Beate Hilbert[1], Vanessa Kirschner[1,2], Sascha Duglosz[4], Frank Zimmermann[4], Marc Freichel[1,2] *, Alex Cornean[1,2] *

[1] Institute of Pharmacology, Heidelberg University, Heidelberg, 69120, Germany
[2] DZHK (German Center for Cardiovascular Research), Partner Site Heidelberg/Mannheim, Heidelberg University, Heidelberg, 69120, Germany
[3] Heidelberg Biosciences International Graduate School (HBIGS), Heidelberg, 69120, Germany
[4] Interfacultary Biomedical Faculty (IBF), Heidelberg University, Heidelberg, 69120, Germany
[5] Present Address: Medizinische Klinik II, Uniklinikum Würzburg, Würzburg, 97078, Germany

* To whom correspondence should be addressed.
Email: alex.cornean@pharma.uni-heidelberg.de.
Correspondence may also be addressed to marc.freichel@pharma.uni-heidelberg.de.

Keywords: adenine base editing, precision editing, mouse modelling, CRISPR/Cas9, hiPS cells

ABSTRACT

Point mutations cause many genetic disorders, but modelling them in organisms is technically challenging. Creating mouse models that mimic these mutations is crucial for establishing a causal relationship between mutations and disease phenotype, thereby supporting the development of therapeutic strategies. Adenine base editors (ABEs) can correct single-nucleotide variants (SNVs) in disease modelling without double-stranded breaks (DSBs) or donor DNA, achieving higher product purity than traditional Cas9 methods. Earlier ABE techniques faced issues like limited targetability, bystander editing, and off-target effects. By combining two editor advancements, we introduced and tested ABE9-SpRY, an improved ABE variant fused with a PAM-flexible SpRY-Cas9 nickase. Our results show that ABE9-SpRY effectively generates three out of four targeted A-to-G mutations in mouse embryos, with significantly fewer off-target effects than ABE8e-SpRY, achieving desired editing efficiencies of up to 96% in individual adult founder mice.ABE9-SpRY also enhances product purity in mouse embryos and human induced pluripotent stem cells (hiPSCs) compared to ABE8e-SpRY. Our findings showcase ABE9-SpRY's precision and versatility, highlighting it as a powerful tool for accurate *in vivo* point mutation modelling.

INTRODUCTION

Disease models have been indispensable in advancing biomedical research by enabling the study of complex physiological and biological interactions that are difficult to replicate *in vitro* [1]. The mouse has emerged as the dominating biomedical model due to its genetic, biological, and behavioural similarities to humans, along with the availability of advanced genetic tools for manipulation [2]. Moreover, mouse models with disease-relevant mutations or mutations in a given drug receptor have tremendous value for the development and validation of the mode of action of new therapies [3-5]. In parallel, hiPSCs have also become a powerful *in vitro* model, providing a human-specific system for studying disease mechanisms, drug responses, and genetic modifications in a physiologically relevant context [6].

The recent development of precise CRISPR/Cas-based gene editing tools has significantly expanded the possibilities for creating genetically engineered mouse models. Notably, the CRISPR/Cas9 system has enabled precise gene modifications by inducing DSBs at specific genomic loci [7]. Its efficiency, widespread adaptation and simplicity have made CRISPR/Cas9 the most widely used system for gene editing. However, the CRISPR/Cas9 system has its limitations. The requirement for DSBs introduces risks such as off-target effects and the formation of insertions or deletions (indels) due to the predominant non-homologous end-joining (NHEJ) repair pathway, which can unintentionally disrupt the targeted site or introduce unintended mutations elsewhere [8,9]. Likewise, larger deletions [10] and chromosomal aberrations [11] have been reported to occur at significantly higher frequencies with DSB-inducing genome editing approaches.

To address the limitations of DSBs, DNA base editing has emerged, which is catalysed by a new class of tools known as base editors [12,13]. Base editors allow single nucleotide conversions without needing DSBs or donor DNA templates. ABEs are of particular interest for introducing A-to-G (or T-to-C) base transitions [12], which are relevant to a wide range of genetic disorders. For example, G•C to A•T mutations account for approximately 47% of the most common pathogenic SNPs in the ClinVar database [14]. By fusing a Cas9 nickase (Cas9n) with a deaminase enzyme that converts adenine to inosine, then read as guanine by the cell, ABEs have been used to install point mutations with high efficiency and precision [12,15].

ABEs, therefore, hold immense promise for enabling the rapid and precise generation of disease models in animal and cell models, especially in mice. However, current ABE approaches in mice are limited by bystander editing, issues of targetability and off-target (OT) editing **(Fig. 1)**. Bystander editing occurs when nucleotides within the editing window of the deaminase, other than the target site(s), are also edited [14], leading to unwanted mutations and making it difficult to study the disease mutations specifically. Canonical ABEs are also limited by their dependency on the NGG protospacer adjacent motif (PAM) recognised by the commonly used *Streptococcus pyogenes* Cas9 nickase, restricting the

range of targetable sites in the genome [12]. Both Cas-dependent, guided by the sgRNAs' base pairing properties to similar genomic regions [16,17], and Cas9-independent off-target editing, based on deaminase activity on adenines in single-stranded DNA regions outside the targeted site [18,19], have raised serious concerns. These limitations have driven efforts to improve ABEs through directed evolution and rational design. Next-generation variants, such as ABE8e [20], exhibit enhanced deaminase activity, whereas ABE9 has increased specificity due to a narrower editing window [21]. Additionally, engineered Cas9 variants like SpRY, which have relaxed PAM requirements, have expanded the range of targetable sequences, allowing for more flexible editing across the genome [22]. We therefore aimed to combine the specificity of the ABE9 deaminase with the flexibility of SpRY, thereby overcoming all three challenges and benchmarking these against ABE8e-SpRY [23], to establish four different mouse models with precise point mutations in the ion channels TPC1, TPC2, and TRPM4. These channels play critical roles in physiological processes, and mutations in these channels have been linked to diseases, particularly affecting hepatic and cardiovascular tissues [24-28].

To streamline the generation of disease models in mice and substantially reduce the number of required animals, we established a workflow to characterise and employ ABE9-SpRY for the rapid introduction of desired mutations. After initial benchmarking and strategy design, we cloned and tested the desired sgRNA/ABE-SpRY combinations in N2a cells, followed by pooled injection of synthetic sgRNAs and SpRY-ABEs mRNA into mouse zygotes and analysis of all target and selected OT sites in E14 embryos. Our strategy enabled generating two point mutation mouse models in the absence of bystander editing and with high efficiency for *Tpc1*^{I486T} and *Trpm4*^{L903P}, which can, due to its broad targetability, be used to create a substantial fraction of A-to-G-based mouse models.

RESULTS

Efficient and precise A-to-G base editing with ABE9 in human cells

The most widely used ABE variant today is ABE8e, recognised for its high deaminase activity and processivity [20]. However, the increased catalytic activity coincides with a significant broadening of the editing window, expanding from adenine positions A4-A8 in ABEmax to A3-A10 in ABE8e [29], as well as higher levels of off-target DNA and RNA editing [20,21,29]. Therefore, this rise in unwanted on-target bystander and off-target editing raises concerns regarding the safety of ABE8e for potential clinical applications [29]. To address these safety concerns, several approaches have frequently been employed in the past (**Table 1**): introducing structure-guided or evolved mutations in the deaminase domain [15,20,21,29-33], splitting the editor [34,35], using low mismatch tolerance Cas variants [36], and fusing the ABE with an effector domain [37].

Among all these options, ABE9, which was derived from ABE8e by introducing two point mutations N108Q and L145T in the deaminase domain, appeared to be the most suitable due to its narrowest editing window to date, located between protospacer positions 5-6, and its strong properties for reducing off-target effects in DNA and RNA [21]. To this end, we compared ABE8e and ABE9 at four previously reported ABE target sites in HEK293T cells to confirm their properties (**Supplementary Fig. 1**). Indeed, the editing window of ABE9 was specific to positions A5 and A6, with some minimal activity at A4, whereas ABE8e was highly active between A3 and A8 with an extended activity shoulder to A13. Overall, the average activity at A5 was reduced from 43.6 ± 5.9% (mean±s.d.%) in ABE8e to 34.5 ± 8.8% in ABE9, corresponding to an average reduction of 21% in editing activity, in line with previous work [21] (**Supplementary Fig. 1**). We were, therefore, able to confirm the potential of ABE9 and, encouraged by this, proceeded to apply its precision to our loci of interest.

ABE9-SpRY is a precise and versatile editor in mouse cells

We first designed the sgRNAs for the four loci to position the target adenines within the optimal editing windows of the deaminases of ABE8e and ABE9, respectively (**Fig. 2a**). However, the canonical architectures of PAM-interacting motifs in both ABEs, when fused to the standard *Sp*Cas9n, proved unsuitable due to the lack of the NGG PAM sequence.

To address this limitation, we next considered alternative Cas9 variants that have different or relaxed PAM requirements, including *Sa*Cas9, xCas9, *Sp*Cas9-NG, *Sp*Cas9-VQR, and SpRY [22,38-43]. Instead of an "on-demand" context-dependent approach, we developed a versatile editing strategy that can be applied to all four loci of interest by utilising a single construct and the appropriate sgRNA. SpRY [22] and SpRYc [44] have emerged as potentially universal Cas9 variants with PAMless targetability across NNN PAMs (**Table 1**). SpRY stands out for having the broadest and most relaxed PAM compatibility

124 and has previously been tested with ABE8e variants [31-33]. We fused a SpRY nickase (in the following
125 simply "SpRY", bears these substitutions compared to *Sp*Cas9 nickase:
126 A61R/L1111R/D1135L/S1136W/G1218K/E1219Q/N1317R/A1322R/R1333P/R1335Q/T1337R) to
127 the TadA domains of ABE8e or ABE9 to streamline the experimental workflow and maximise the
128 potential for successful genome editing outcomes (**Fig. 2b**). These SpRY base editors can, in theory,
129 effectively target spacers with NRN (G or A) PAMs, and to a lesser degree, NYN (T or C) PAMs [22].

130 Since the compatibility of deaminase domains with Cas9 variants is not universal, and their efficiency
131 and editing activity can vary based on the specific Cas9 variants used [15,45,46], an initial evaluation was
132 necessary. Due to the lack of published reports on ABE9-SpRY, we compared it to ABE8e-SpRY using
133 a plasmid-based lipofection approach alongside the respective sgRNAs for the four loci of interest in
134 mouse Neuro-2a (N2a) cells (**Fig. 2c**).

135 Deep sequencing of transfected cells revealed that the desired editing occurred at all four targets for
136 ABE8e-SpRY, ranging from 14.1 ± 0.7% to 60.6 ± 1.2%. In contrast, only three targets showed targeted
137 A-to-G editing with ABE9-SpRY, ranging from 6.5 ± 0.9% to 13.2 ± 1.5% across all tested sites
138 (**Fig. 2d**). While ABE8e-SpRY displayed modest editing of 14.1 ± 0.7% at the *Tpc2-K188* locus, no
139 desired editing was noted with ABE9-SpRY. A closer examination of editing at adenines within the
140 sgRNA target sites confirmed the previously observed broad activity window of ABE8e-SpRY, which
141 included 13.5 ± 0.5% editing at A2 and 20.8 ± 0.6% editing at A12 at the *Tpc1-I486* locus (**Fig. 2e**).
142 The highest ABE8e-SpRY activities were observed at A5 (*Tpc2-K188*, *Tpc2-L249*, *Trpm4-L903*) and
143 A6 (*Tpc1-I486)*, with 30.8 ± 0.5%, 26.1 ± 6.5%, 41.9 ± 12.8%, and 61.6 ± 12.7% A-to-G editing,
144 respectively. By contrast, ABE9-SpRY demonstrated the enhanced precision previously observed for
145 ABE9, with the activity window spanning from A4 to A9 at the *Tpc1-I486* locus, showing 9.1 ± 1.3%
146 and 3.3 ± 0.5% editing, respectively. We also measured the highest efficiencies for ABE9-SpRY at A5
147 and A6, respectively, with 6.5 ± 0.9%, 12.8 ± 0.8%, and 13.7 ± 1.7% efficiency for *Tpc2-L249*, *Trpm4-*
148 *L903*, and *Tpc1-I486,* respectively. This narrower editing window of ABE9-SpRY also led to a larger
149 fraction of edited alleles containing no bystander mutations compared to ABE8e-SpRY (**Fig. 2f**), as
150 indicated by the substantially higher product purity, ranging from 50.9 ± 2.4% to 98.6 ± 0.6%,
151 compared to 1.1 ± 0.1% to 69 ± 0.8% for ABE8e-SpRY (**Fig. 2g**). Notably, the desired $Tpc1^{I486T}$ and
152 $Trpm4^{L903P}$ mutations could not be introduced without bystanders using ABE8e-SpRY (0.7 ± 0.1% and
153 0.5 ± 0.3%), whereas ABE9-SpRY achieved 6.7 ± 0.4% and 11.9 ± 1.4% precise editing at these sites,
154 respectively. Lastly, ABE9-SpRY demonstrated reduced indel frequencies compared to ABE8e-SpRY
155 across all four sites, peaking at 0.9 ± 0.2% (*Tpc1-I486*) (**Fig. 2h**).

156 Taken together, these *in vitro* results for ABE target sites in mouse cell line indicated that ABE9-SpRY
157 can precisely edit three out of four desired target sites, two of which could not be generated with ABE8e-

158 SpRY due to bystander mutations. Therefore, we next decided to apply these approaches *in vivo*, testing
159 editing efficiencies in mouse embryos.

160 **Multiplexed, precise ABE9-SpRY mouse embryo editing**

161 Adenine base editing in mouse zygotes has been successfully performed using a combination of ABE
162 mRNA and either *in vitro* transcribed or chemically synthesised modified sgRNAs, injected into the
163 cytoplasm or pronucleus of the zygote [37,47-52]. Indeed, these efforts have been highly efficient in
164 achieving nearly 100% editing using ABE7.10 [47-49]. However, precision issues were apparent, as only
165 1.3% to 20% of desired edits occurred within an overall A-to-G efficiency of 95% in the protospacer
166 [48].

167 To evaluate the *in vivo* editing efficiency of our approach in mouse embryos, we microinjected a pool
168 of four synthetic sgRNAs along with either *in vitro* transcribed ABE8e-SpRY or ABE9-SpRY mRNA
169 into the cytoplasm of mouse zygotes. The injected zygotes were transferred to pseudopregnant surrogate
170 mothers, isolated on embryonic day 14, and their genomic DNA was extracted for targeted deep
171 sequencing analysis (**Fig. 3a**).

172 Our analysis indicated that ABE8e-SpRY effectively edited target adenines at all four sites, achieving
173 editing efficiencies of up to 100%. The average editing efficiencies were 78.9 ± 25.7% at *Tpc1-I486*
174 [median (IQR), 91.4% (67.0-99.9%)], 52.6 ± 30.8% at *Tpc2-K188* [median (IQR), 54.5% (32.9-70.1%)],
175 84.5 ± 20.2% at *Tpc2-L249* [median (IQR), 94.1% (75.1-99.9%)], and 99.8 ± 0.6% at *Trpm4-L903*
176 [median (IQR), 99.9% (41.7-100.0%)], (**Fig. 3b**). Editing by ABE9-SpRY was observed at *Tpc1-I486T*,
177 *Tpc2-L249*, and *Trpm4-L903P*, achieving efficiencies of up to 59.1%, 62.3%, and 89.3%, with
178 corresponding averages of 11.0 ± 18.1% [median (IQR), 0.04% (0.02-20.26%)], 11.9 ± 16.8% [median
179 (IQR), 6.71% (0.04-12.95%)], and 23.7 ± 28.6% [median (IQR), 8.50% (0.03-48%)], respectively.

180 A closer examination of adenine base editing across the protospacer sequences revealed a pattern
181 consistent with previous *in vitro* findings. Despite the high editing efficiency of ABE8e-SpRY, its
182 activity was broadly distributed, targeting adenines from positions A2 to A14 across all tested loci
183 (**Fig. 3c**). In contrast, ABE9-SpRY exhibited a narrower editing window, concentrating edits primarily
184 within positions A4 to A8. Notably, low-level editing was detected in a single embryo at the *Tpc2-K188*
185 locus, where ABE9-SpRY had shown no *in vitro* activity. This editing occurred at only one of the two
186 targeted adenines, resulting in a 25.2% conversion that introduced a p.K188E substitution instead of the
187 intended p.K188G mutation.

188 ABE9-SpRY exhibited a higher rate of desired edits with no bystander edits at the *Tpc1-I486* locus
189 (10.7 ± 17.5% vs 0.3 ± 1.2%) and at *Trpm4-L903* (21.3 ± 28.4% vs 0.0 ± 0.0%). In contrast, ABE8e-
190 SpRY showed more specific activity at *Tpc2-K188* (25.5 ± 25.9% vs 0.0%) and *Tpc2-L249* (52.8 ± 27.5%

191 vs 11.8 ± 16.2%) (**Fig. 3d**). Analysing product purity as a measure of precision revealed that ABE9-
192 SpRY generated significantly purer editing outcomes across all active loci: *Tpc1-I486* (85.1 ± 30.6%
193 vs 1.2 ± 5.3%), *Tpc2-L249* (94.6 ± 22.3% vs 60.8 ± 27.1%), and *Trpm4-L903* (90.5 ± 20.8% vs 0.0%)
194 (**Fig. 3e**). Furthermore, ABE9-SpRY produced only low levels of indels, similar to ABE8e-SpRY
195 (**Fig. 3f**).

196 Only one C-to-T conversion was noted at the *Tpc1-I486* locus in an embryo edited with ABE8e-SpRY,
197 occurring at a frequency of 12.6% at position C6, alongside a single instance of 34.7% unwanted A-to-
198 C editing (**Supplementary Fig. 2a**). Additionally, an unexpected off-target modification was found
199 upstream of the sgRNA binding region at position A-2 of the *Tpc2-L249* locus
200 (**Supplementary Fig. 2b**). This edit appeared in one ABE9-SpRY and one ABE8e-SpRY injected
201 embryo at frequencies of 12.3% and 21.9%, respectively. A possible explanation is the dynamic nature
202 of the Cas9-sgRNA-DNA complex and conformational changes during editing, which may briefly
203 expose adjacent bases to the deaminase domain, leading to unintended deamination events.

204 These findings suggest that ABE9-SpRY provides enhanced editing purity, though it does so at the
205 expense of locus-dependent activity. To further assess precision beyond these target loci, we next
206 analysed both Cas9-dependent and Cas9-independent off-target editing to more thoroughly characterise
207 the safety profiles of these two editors.

208 **ABE9-SpRY substantially decreases off-target effects compared to ABE8e-SpRY**

209 Cas-dependent off-target events arise from the tolerance of mismatches between sgRNA and the
210 targeting sequence. Although SpRY can target a broader range of genomic sites, its relaxed PAM
211 tolerance also implies that the potential Cas-dependent off-target sites are substantially expanded, as
212 sgRNA-DNA mismatches become the sole determinant of off-target binding without PAM constraints.
213 Consequently, we identified the top five predicted off-target sites for each locus using ACEofBASEs [53]
214 and analysed these sites across three embryos per group.

215 When analysing the cumulative percentage of reads containing edits in the off-target spacer sequences,
216 we found that the average cumulative A-to-G editing in the off-target protospacer at the *Tpc1-I486* off-
217 target sites varied from 4.1 ± 5.7% to 264.3 ± 15.6% for ABE8e-SpRY, compared to baseline control
218 levels for ABE9-SpRY (**Fig. 4a, Supplementary Fig. 3**). Off-target editing at the highest edited
219 adenines ranged from 4.1 ± 7.0% at OT2 to 27.8 ± 17.4% at OT3 for ABE8e-SpRY
220 (**Supplementary Fig. 3**). Overall, across 20 off-target sites with various PAM sequences, ABE8e-
221 SpRY induced A-to-G edits above control levels at 14 sites, especially at protospacer positions A2 to
222 A20 (**Fig. 4a–d, Supplementary Fig. 3–6**). In contrast, ABE9-SpRY edited just two off-target sites
223 associated with the *Tpc2-L249* locus, reaching 40.0% and 48.1% editing, respectively (**Fig. 4c,**
224 **Supplementary Fig. 5**). Strikingly, for these two off-target sites, the corresponding embryos' on-target

editing efficiencies at the locus were relatively low, at 7.4% and 10.7%. While off-target effects are known to occur with base editors, this drastic skew towards off-target editing (with a 3-base mismatch) is remarkable. Since these events were observed in just one replicate of ABE9-SpRY, the data indicate that ABE9-SpRY is a notably improved precision tool, though rare, sequence-dependent off-target activity may still occur.

In addition to Cas-dependent off-target effects, base editors have also been reported to exhibit Cas-independent off-target activity, which is evoked by the deaminase activity of the editors [18,19]. We therefore asked whether TadA-8e and TadA-9 deaminases cause Cas-independent off-target effects to similar extents, regardless of the Cas9 nickase variant to which they are attached. To this end, we utilised the orthogonal R-loop assay [54] (**Fig. 4e**) in HEK293T cells and, after FACS-enrichment of GFP co-transfected cells, observed no editing across eight adenines and three R-loop spacers with ABE9-SpRY, similar to the results reported earlier for ABE9 [21]. In contrast, ABE8e-SpRY caused substantial editing from 4.3 ± 1.1% (R loop 1), 7.7 ± 2.7% (R loop 2), to 12.0 ± 1.4% (R loop 3). These results highlight the high specificity of ABE9-SpRY despite the increased non-specific binding of SpRY.

ABE9-SpRY is effective at generating precise *Tpc1*^{I486T} and *Trpm4*^{L903P} founder mice

Accurate base conversion is crucial for modelling SNVs; therefore, minimising bystander and off-target mutations is essential. Given the negligible levels of bystander editing, low Cas9-dependent off-target editing, and no evidence above background of Cas9-independent off-target editing produced by ABE9-SpRY, we decided to use this editor for generating two individual founder mouse lines harbouring the *Tpc1*^{I486T} and *Trpm4*^{L903P} mutations. To achieve this, ABE9-SpRY and the locus-specific sgRNAs were injected separately into mouse zygotes. Analysis of adult mice biopsies from 48 putative F0 founder mice revealed robust editing efficiencies (**Fig. 5a,b**), with the precise, bystander, and indel-free p.I486T achieved at 25.6 ± 21.0% efficiency [median (IQR), 26.1% (4.9-44.7%)], and up to 81.4% (**Fig. 5b**). The very low rate of bystander editing at A4 (**Fig. 5b**) resulted in a considerable product purity of 96.4 ± 13.8% [median (IQR), 98.9% (98.8-99.0%)] (**Fig. 5c**). While one individual mouse exhibited an indel frequency of 11.2% at the *Tpc1-I486* locus, overall indel levels were generally minimal (0.3 ± 1.6%). Analysis of 36 *Trpm4-L903* ABE9-SpRY edited mice showed a similar trend (**Fig. 5d,e**). The product purity was comparable, as observed for *Tpc1-I486*, at 93.9 ± 10.3% [median (IQR), 97.6% (97.4-97.8%)] (**Fig. 5f**), due to the limited bystander editing events at A8 (**Fig. 5c**). Overall, p.L903P was accurately and precisely established at even higher efficiencies than p.I486T, at frequencies of 28.3 ± 20.8% [median (IQR), 21.2% (10.4-34.7%)], and up to 96.0% (**Fig.5e**). Similarly, indel frequencies were slightly higher at the *Trpm4-L903* locus at 1.0 ± 5.9%, reaching 35.5% in one instance.

To determine the F1 transmission rate and establish stable mutant lines for *Tpc1* p.I486T and *Trpm4* p.L903P, we proceeded to mate two verified adult F0 *Tpc1* p.I486T male mice **(Fig. 5b)** and three verified adult F0 *Trpm4* p.L903P male mice **(Fig. 5e)** with wild-type females. We observed high

transmission rates for *Tpc1* p.I486T of 55.6% and 62.5% in the two independent matings **(Fig. 5g, Supplementary Fig. 7a)**, and high to complete transmission for *Trpm4* p.L903P at rates ranging from 80% to 100% **(Fig. 5h, Supplementary Fig. 7b)**. Finally, we mated select heterozygous F1 carriers with wild-type mice to establish stable lines (**Supplementary Fig. 8).**

These results suggest that the pooled embryo analysis has somewhat underestimated the potential editing efficiency of ABE9-SpRY when deployed to individual loci rather than diluted across several for screening. Moreover, the highly precise editing rates and encouraging off-target profile indicate the potential for direct founder-generation phenotyping, which could accelerate experimental timelines and reduce both resource consumption and the number of animals required.

Precise hiPSC engineering with ABE9-SpRY

Over the past two decades, hiPSCs have become a powerful *in vitro* model, offering a human-specific system for studying disease mechanisms, drug responses, and genetic variants in a physiologically relevant context when paired with directed-differentiation procedures [55,56]. Given this importance, we aimed to validate the potential of ABE9-SpRY for disease modelling in hiPSCs. To enrich base-edited cells, we used the XMAS-TREE assay [57], in which a successful A-to-G conversion of a stop codon in between an episomal mCherry-linker-EGFP construct leads to the co-expression of GFP alongside the pre-existing mCherry signal (**Fig. 6a**). We selected the human p.I485T mutation of human *TPC1*, corresponding to mouse *Tpc1* p.I486T, as a test and designed two sgRNAs with the target adenine located either in position A5 (sgRNA#2) or A6 (sgRNA#1) of the protospacer sequence, respectively (**Fig. 6b**). We then co-transfected either ABE8e-SpRY or ABE9-SpRY plasmid, which we re-cloned under an EF1α promoter for robust hiPSC expression, along with the reporter plasmid, a reporter-STOP-sgRNA plasmid, and either of the two target sgRNA plasmids, thereby enriching the base-edited cell population through FACS sorting (**Fig. 6c**). While the overall editing efficiency was substantially higher with ABE8e-SpRY, 75.8 ± 1.0% editing with sgRNA#1 and 33.7 ± 2.0% with sgRNA#2, ABE8e-SpRY was also active very broadly. In particular, the two adjacent bases A4 and A6, or A3 and A5 for sgRNA#1 and sgRNA#2, respectively, displayed very similar activity. By contrast, ABE9-SpRY achieved efficiencies of only up to 10.9 ± 0.7% (**Fig. 6d**). However, we observed superior overall desired editing activity without unwanted mutations, a result of the higher precision, with sgRNA#1 reaching 9.9 ± 0.7%. Notably, despite ideal target site positioning, sgRNA#2 showed a slightly lower efficiency at 7.6 ± 0.6% (**Fig. 6e**). The highest editing rate without unwanted mutations for ABE8e-SpRY was 3.0 ± 0.1%. While the overall editing rates of ABE9-SpRY were lower, this limitation is less critical in the context of hiPSC-based disease modelling, where correctly edited clones are typically isolated and expanded prior to downstream differentiation into specific cell types of interest. Importantly, such clonal isolation strategies rely on the high precision of the editing event, which we achieved with ABE9-SpRY, but not ABE8e-SpRY. In addition to the increased frequency of indels

295 observed (**Fig. 6f**) at 2.9 ± 0.5% with ABE8e-SpRY compared to 0.1 ± 0.1% with ABE9-SpRY using
296 sgRNA#1, these results further bolster the case for the potential of ABE9-SpRY in a wide variety of
297 precision disease modelling applications, spanning from animal to cellular models.

298 **DISCUSSION**

299 Base editing holds great promise for modelling point mutations due to its benefits over existing
300 techniques, as it prevents DSBs and shows high on-target efficiency [12,13]. While previous studies have
301 utilised base editing for animal modelling, they have frequently encountered issues such as off-target
302 effects, bystander editing, and indels [47,48,58,59].

303 Successful disease modelling via base editing requires (1) precise editing with no bystander missense
304 mutations, as they can easily mask or disrupt the interpretation of the desired mutation [60]; (2) absence
305 of indels on the same allele to avoid frameshifts and truncated proteins [61]; and (3) minimal off-target
306 effects, which, if frequent, can persist despite outcrossing [62] and may necessitate costly genome-wide
307 validation.

308 Here, we utilised the latest advancements in the gene editing toolbox to address these issues. We
309 demonstrated that using ABE9, an adenine base editor recognised for its high specificity and safety
310 profile [21], fused with the PAM-less SpRY-Cas9 nickase [22], can efficiently introduce A-to-G mutations
311 with great flexibility. It results in low to no bystander editing, minimal detectable Cas-dependent off-
312 target effects at only two sites, and very few indels, achieving up to 89% precise editing of desired
313 changes in mouse embryos. Moreover, in adult F0 founder mice, we observed up to 96% desired editing
314 at the *Trpm4-L903* locus, highlighting the potential for phenotyping within the same generation. In
315 contrast, ABE8e-SpRY exhibited a higher overall A-to-G conversion efficiency, close to homozygosity.
316 However, this was accompanied by bystander mutations at similar frequencies, resulting in significantly
317 lower product purities. Furthermore, ABE8e-SpRY caused substantial levels of Cas-dependent off-
318 target editing in mouse embryos at 14 of 20 sites examined, with A-to-G editing frequencies at OT5 of
319 the *Trpm4-L903* sgRNA reaching up to 84%. Therefore, the trade-off between reduced editing
320 efficiency and high precision remains a valuable advantage that ABE9-SpRY offers for generating
321 genetic and disease models where bystander editing is unacceptable.

322 We found that pooling sgRNAs during the initial *in vivo* testing in embryos is an effective strategy. This
323 approach enables rapid screening of editing outcomes with reduced effort and decreases the number of
324 animals required. However, this approach seems to underestimate editing efficiency compared to
325 experiments where only a single sgRNA is injected. For example, at the *Tpc1-I486* locus, perfect editing
326 (desired editing without bystander edits) occurred at a frequency of 10.7 ± 17.5% in embryos (pooled)
327 versus 25.6 ± 21.0% in adults (single). Similarly, at the *Trpm4-L903* locus, the desired editing frequency
328 was 21.3 ± 28.4% (pooled) versus 28.3 ± 20.8% (single). This discrepancy may stem from the dilution

329 of the editing machinery across four different target sites, and potentially their off-targets, in the pooled
330 condition. This likely reduces the effective concentration of the editor at each individual locus, thereby
331 lowering the observed editing efficiency.

332 At the *Tpc2-K188* locus, ABE8e-SpRY demonstrated efficient editing, while only one mouse embryo
333 showed any editing for ABE9-SpRY. This indicates that the SpRY-Cas9n protein can access this target
334 site, but the evolved TadA-9 deaminase enzyme has shown reduced substrate acceptance compared to
335 TadA-8e. Given that the N108Q and L145T mutations in ABE9 are speculated to expel the backbone
336 of the DNA substrate [21], this may also change the substrate-interaction behaviour of TadA-9 compared
337 to TadA-8e, in addition to altering the editing window. As such, the observation at the *Tpc2-K188* locus
338 suggests that, in addition to altering the editing window, these mutations may create sequence-
339 dependent steric hindrances that prevent the enzyme from effectively engaging with the target adenine,
340 even within its supposedly optimal editing window. To better understand the genome-wide targeting
341 properties of ABE9-SpRY, a combination of detailed structural analyses to elucidate the mechanisms
342 by which the N108Q and L145T mutations influence substrate binding and high-throughput *in vitro*
343 analysis of a large number of disparate target sites will be required. However, despite its efficiency,
344 ABE8e-SpRY would not be the alternative to ABE9-SpRY in cases such as those at the *Tpc2-K188*
345 locus due to its off-target profile. For sites untargetable by ABE9-SpRY, alternative variants with
346 enhanced specificity, such as ABE8e-WA/WQ [30], ABE8e-N108Q [21], ABE8e-V106W [20], and next-
347 generation ABEs (e.g., ABE8r, ABE-Umax, ABEx2/4, E2-/E4-ABE, TadA-8e-L1B_S116, hpABE5.20
348 [63-68], are emerging and may serve as effective substitutes when fused to SpRY-nickase. In practice, the
349 advent of scalable machine learning-based engineering tools to create bespoke ABE-SpCas9 variants
350 with target-specific PAMs [69] will help to maximise on-target editing by use of the highest activity and
351 precise deaminases with context-specific PAM-interacting motifs, to substantially reduce off-target
352 editing.

353 The PAM-less properties of SpRY, in any combination with next-generation genome editors, present
354 significant challenges of their own, particularly concerning increased off-target genome editing, which
355 consequently leads to a rise in chromosomal rearrangements [11]. As a result, ABE-SpRY editors are
356 expected to demonstrate increased off-target editing due to their ability to bind and modify DNA
357 sequences without the stringent necessity for a PAM. ABE8e-SpRY demonstrated extensive Cas9-
358 dependent off-target editing at 70% of the examined off-target sites. At one of these sites, *Trpm4-L903*
359 OT5, editing reached up to 84%. ABE9-SpRY, in contrast, exhibited editing at only 10% of the
360 examined sites. We acknowledge that a limitation of our off-target analysis is its dependence on *in silico*
361 predictions of potential non-specific sgRNA binding sites. This method may introduce bias, as the sites
362 are selected *a priori* and might miss *bona fide* off-target effects. Nonetheless, it remains a common and
363 practical initial method for evaluating base editor specificity. To complement *in silico* predictions, a
364 suite of unbiased genome-wide off-target detection methods has been developed in recent years [70]. For

365 adenine base editors, specific unbiased genome assays like EndoV-seq (76), Digenome-seq (77), and
366 Selicit-seq (78) have been developed. Especially when stringent validation is necessary, such as in
367 clinical settings, these should be complemented with detailed chromosome-level structural analyses
368 using assays like CAST-seq (80). Although these advanced methods are valuable, our results using *in*
369 *silico* prediction already demonstrate that ABE9-SpRY strikes an attractive balance of precision and
370 flexibility, supporting its suitability for generating disease models.

371 hiPSCs are increasingly utilised for disease modelling because they closely resemble the human genome
372 and can differentiate into specific tissues [71]. As hiPS cell culture continues to advance from traditional
373 2D systems to more intricate 3D models, it enables advanced exploration of pathophysiological
374 mechanisms and disease modelling [72]. For this purpose, reproducing genetic variants as precisely as
375 possible is crucial, making the exclusion of bystander editing and limitation of off-target effects
376 indispensable [73]. Given the target flexibility of ABE9-SpRY, we designed two tiled sgRNAs across the
377 target site and demonstrated that ABE9-SpRY could precisely induce a single-base change in hiPSCs
378 without bystander editing. Although editing efficiency is relatively low compared to ABE8e-SpRY, and
379 clonal isolation remains necessary for certain downstream gene mutation studies, the absence of
380 bystander editing simplifies the clonal isolation. Utilising reporter assays for editing enrichment, such
381 as XMAS-TREE, and optimising the delivery method will help overcome the limitations of low editing
382 efficiencies [74,75].

383 Overall, ABE9-SpRY demonstrates high precision while maintaining considerable flexibility, which is
384 crucial, as missense mutations can be highly detrimental. For example, in the context of disease rescue,
385 even with ABE8e's high efficiency in introducing the intended point mutation, a bystander edit caused
386 a missense mutation that ultimately prevented phenotypic rescue [60]. This underscores the importance of
387 precision editors like ABE9-SpRY, particularly when modelling diseases or designing therapeutic
388 strategies where functional outcomes are paramount. This level of precision is essential for fundamental
389 research, such as structure-function studies of a specific protein domain, where even a single unintended
390 amino acid change introduced by bystander editing could make the results uninterpretable. The potential
391 for base editors to introduce confounding SNVs, as systematically demonstrated in mouse embryos [59],
392 underscores the need for cleaner tools like ABE9-SpRY to produce reliable models for functional
393 analysis. With ABE9-SpRY's versatility in targeting specific adenines, along with minimised bystander
394 editing and reduced Cas-dependent and Cas-independent off-target effects, it represents a valuable tool
395 for creating precise disease models in both animals and cell lines, hiPSCs, and organoids derived from
396 them.

397 **METHODS**

398 All methods were performed in accordance with the relevant guidelines and regulations.

399 **Reagents and biological resources**

400 Information on major resources is provided in **Supplementary Table 1**.

401 **Mouse strains**

402 Wild-type C57BL/6N mice were purchased from Charles River Laboratories (Wilmington, MA, USA).
403 The experimental procedures were approved by the regional council of Karlsruhe, Germany, in
404 accordance with the Animal Welfare Act (AZ35-9185.81/G-60/23). Microinjection was performed in
405 the cytosol of C57BL/6N zygotes. All animals were housed in the Interfaculty Biomedical Faculty (IBF)
406 of Heidelberg University. Mice were maintained under specified pathogen-free conditions with a 12-
407 hour light/12-hour dark cycle, and water and standard food (Rod18, LASvendi GmbH, Germany)
408 available ad libitum. All mouse experiments described in this study comply with ARRIVE guidelines.

409 **Identification and Alignment of Mouse Orthologues for Targeted Point Mutations**

410 To identify the corresponding mutations in the mouse genome, to four target loci of interest with
411 missense mutations *Tpc1 p.I485T*, *Tpc2 p.L265P*, *Tpc2 p.K204A*, and *Trpm4 p.L907P* we retrieved the
412 *Mus musculus* and *Homo sapiens* gene sequences from Ensembl and performed protein sequence
413 alignments. This allowed us to pinpoint the target amino acids and the corresponding adenines in the
414 mouse coding sequence. Through this alignment, we identified the orthologous amino acid residues in
415 the respective mouse genes and the potential missense mutations we can model by A-to-G transition
416 mutation mediated through ABEs: *Tpc1 p.I486T*, *Tpc2 p.L249P*, *Tpc2 p.K188G*, and *Trpm4 p.L903P*.
417 Notably, for *Tpc2 p.K188G*, a glycine substitution was created *in silico* instead of the alanine. We
418 decided to proceed with the glycine substitution based on the similar chemical and functional properties
419 of glycine and alanine.

420 **Design and cloning of sgRNAs**

421 sgRNAs were designed manually to enable the precise installation of the defined missense mutations
422 and validated using ACEofBASEs [53] with the following parameters: select BaseEditor "custom ABE"
423 with Window start "3" and Window end "11" with PAM "NRN" for *Tpc1-I486*, *Tpc2-K188*, and *Trpm4-*
424 *L903* target sites or with PAM "NYN" for the *Tpc2-L249* target site; for Species "Mouse (Mus musculus)
425 Ensembl V 103". The full list of sgRNA oligonucleotides to clone and the sgRNAs used in this study
426 are shown in Supplementary Tables 2 and 3.

427 For *in vitro* applications of sgRNAs, the 20 bp *Sp*Cas9 sgRNA spacer sequences used in this study were
428 designed with the 5' and 3' sequences (**Supplementary Table 2**), as previously described [76], with an
429 additional 5' "G" added in cases in which the spacer does not start with a G. In brief, the 20 bp target
430 site (N20) sequences were ordered as oligonucleotides with the following sequences 5'-CACC(N20-
431 21)GTTTT-3', while the sequences complementary to the target site were designed and ordered as
432 oligonucleotides as follows 5'-CTCTAAAAC(N20-21)-3'. sgRNAs were cloned into the BsaI-digested
433 2.18 kb pU6-pegRNA-GG-acceptor fragment (pU6-pegRNA-GG was a gift from David Liu, Addgene
434 plasmid #132777, [76]) by oligonucleotide annealing and Golden Gate assembly as previously described
435 [76], including the standard *Sp*Cas9 sgRNA scaffold.

436 *R-loop SaCas9 sgRNAs.* To generate the *Sa*Cas9 sgRNA plasmid, BPK1520, containing a
437 pU6_BsmBIcassette-Sp-sgRNA was used as a backbone (BPK1520 was a gift from Keith Joung,
438 Addgene plasmid #65777, [39]). The *Sp*Cas9 sgRNA scaffold was digested using *BsmBI* and *HindIII*, and
439 the digested fragment was isolated. The *Sa*Cas9 sgRNA scaffold sequence [42], designed with
440 complementary overhangs (**Supplementary Table 2**), was ligated into the digested vector backbone.
441 The designed sgRNA spacer sequences were then ordered as oligonucleotides with *BsmBI* overhangs
442 (**Supplementary Table 2**), and the annealed oligos were cloned into the *BsmBI*-digested *Sa*Cas9
443 sgRNA plasmid via Golden Gate assembly. In brief, in a 10 µl reaction volume, 50 ng of *Sa*Cas9 sgRNA
444 plasmid, 10 units of *BsmBI*-v2 (NEB), 20 units of T4 DNA ligase (NEB), 1 µL of 1 µM annealed spacer
445 oligonucleotides, 1X T4 DNA ligase buffer were assembled under the following thermal cycling
446 conditions: digestion at 42°C for 4 minutes, followed by ligation at 16°C for 3 minutes, repeated for a
447 total of 11 cycles. The reaction was then incubated at 80°C for 10 minutes to inactivate *BsmBI*.

448 *hiPSC sgRNAs.* Cloning of targeting sgRNA into the pDT-sgRNA-XMAS-1x plasmid was performed
449 as previously described (pDT-sgRNA-XMAS-1x was a gift from Xiao Wang, Addgene plasmid
450 #164413, was performed as previously described [57]).

451 All sgRNAs for mouse experiments were ordered via Integrated DNA Technologies (IDT) as custom
452 Alt-R CRISPR-Cas9 sgRNA (**Supplementary Table 3**).

453 **Cloning of adenine base editor plasmids**

454 All plasmids constructed here were cloned via Gibson Assembly using the NEBuilder HiFi DNA
455 Assembly (NEB) kit with PCR products amplified from designated template plasmids with specific
456 primers (**Supplementary Table 4**) with Q5 Hot Start DNA polymerase (NEB).

457 To obtain pCMV_ABE9, we used the ABE9 editor sequence form [21], and recloned pCMV_ABE8e (a
458 gift from David Liu, Addgene plasmid #138489, [20]) by introducing the two defining mutations N108Q
459 and L145T by PCR, altogether assembled via four fragments (**Supplementary Table 4**):

460 pCMV_backbone, ABE9_fragment_1_TadA*_Nterm_N108Q,
461 ABE9_fragment_2_TadA*_N108Q_L145T, ABE9_fragment_3_Cas9n-Nterm. To clone
462 pCMV_ABE8e-SpRY, we assembled the following PCR products: pCMV_backbone,
463 ABE8e_fragment1_TadA*, and ABE9-SpRY_fragment_4_SpRY-Cas9n (amplified from pCMV-T7-
464 ABE8e-nSpRY-P2A-EGFP (KAC1069), a gift from Benjamin Kleinstiver, Addgene plasmid #185912,
465 [77]). Similarly, pCMV_ABE9-SpRY was constructed by assembling: pCMV_backbone,
466 ABE9_fragment_1_TadA*_Nterm_N108Q, ABE9_fragment_2_TadA*_N108Q_L145T,
467 ABE9_fragment_3_Cas9n-Nterm, and ABE9-SpRY_fragment_4_SpRY-Cas9n.

468 For the transfection of hiPSCs, pCMV_ABE8e-SpRY and pCMV_ABE9-SpRY were recloned to be
469 expressed under the control of the EF1α promoter. In brief, two fragments were amplified, first the
470 pEF1α_backbone (from pEF1α-hMLH1dn, a gift from David Liu, Addgene Plasmid #174824, [78]) and
471 then either ABE8e-SpRY or ABE9-SpRY, for subsequent Gibson assembly cloning.

472 The entire sequence of all constructs assembled using PCR was verified with the PlasmidEZ
473 (Azenta/GeneWiz) full-plasmid sequencing service. All plasmids used for the transfection experiments
474 were prepared using the EndoFree Plasmid Maxi Kit (Qiagen).

475 **Generation of adenine base editor mRNA**

476 mRNA for the microinjection of mouse zygotes for ABE8e-SpRY and ABE9-SpRY was generated by
477 *in vitro* transcription from *SalI*-HF linearised pCMV_ABE8e-SpRY and pCMV_ABE9-SpRY plasmid
478 templates, respectively, using the HiScribe T7 ARCA mRNA Kit. The mRNA was purified using the
479 RNeasy Mini Kit. mRNA quality was confirmed using the TapeStation RNA ScreenTape.

480 **Mammalian cell culture and transfection**

481 Human HEK 293T cells and Neuro2a cells were purchased from ATCC and maintained in Dulbecco's
482 modified Eagle's medium (DMEM; Gibco) supplemented with 10% FBS (Gibco) at 37 °C with 5 %
483 CO_2, up to 20 passages, by passaging cells every two to three days. hiPSCs were purchased from
484 Greenstone Biosciences and cultured on hESC-Qualified Matrix Matrigel-coated (Corning) 6-well
485 plates (Sarstedt) in StemMACS PSC-Brew XF medium (Miltenyi Biotec). Medium was changed daily,
486 and cells were passaged every three days using StemMACS Passaging Solution XF (Miltenyi Biotec).
487 The culture medium was supplemented with 2.5 µM Rock Inhibitor (Y27632, Miltenyi Biotec) on
488 passaging days for 24 hours. The supernatant media from cell cultures were routinely analysed for
489 mycoplasma presence using the MycoSPY Master Mix (Biontex).

490 All HEK293T and N2a transfection experiments were conducted with at least three independent
491 biological replicates. HEK293T and N2a cells were seeded at a density of roughly 110,000 and 180,000
492 cells per well in 24-well plates, respectively, 20-24 hours before transfections. Transfections were

493 performed with 750 ng of base editor plasmid, 250 ng of sgRNA expression plasmid, and, for
494 experiments involving GFP co-transfection, 200 ng of pMAX-GFP (Lonza), combined with 2 µl of
495 Lipofectamine 2000 (Thermo Fisher Scientific) in a total volume of 50 µl Opti-MEM (Thermo Fisher
496 Scientific), according to the manufacturer's instructions. Medium was exchanged to culture medium
497 approximately 24 hours after transfection. For the Orthogonal R-loop assay, HEK293T cells were
498 seeded at a density of 110,000 cells per well in 24-well plates, as described above. However, the cells
499 were co-transfected with a mixture containing 500 ng of plasmids encoding base editor plasmids, 350 ng
500 of *Sp*Cas9 sgRNA (*HEKsite2*), 500 ng of d*Sa*Cas9, 350 ng of *sa*Cas9 sgRNAs targetting separate
501 genomic loci unrelated to the on-target site, and 200 ng of pMAX-GFP (Lonza).

502 hiPSCs were seeded on 6-well plates and transfected after approximately 24 hours at around 60 %
503 confluency. Before transfections, the medium was changed to StemMACS PSC-Brew XF supplemented
504 with StemMACS PSC-Support XF (Miltenyi Biotec). Transfections were performed with 300 ng
505 pEF1α-XMAS-1xStop (a gift from Xiao Wang, Addgene plasmid #164411, [57]), 300 ng pU6-SpCas9-
506 XMAS-1x plasmid, 2100 ng of pEF1α_ABE8e-SpRY or pEF1α_ABE9-SpRY, and 10 µl
507 Lipofectamine Stem (Thermo Fisher Scientific) per well, according to the manufacturer's instructions.
508 Medium was exchanged to culture medium approximately 24 hours after transfection.

509 **Fluorescence-activated cell sorting**

510 Approximately 48 hours after transfections, HEK293T, N2a or hiPSCs were harvested for sorting.
511 HEK293T and N2a cells were treated with TrypLE Express Enzyme (Thermo Fisher Scientific) to
512 singularise the cells, followed by a washing step with D-PBS. The cells were resuspended in buffer
513 containing 1x PBS without Mg^{2+}/Ca^{2+} (Thermo Fisher Scientific), 0.5% FCS (Thermo Fisher Scientific)
514 and 1% Penicillin-Streptomycin and filtered through a 35 µm cell strainer (Corning). hiPSCs were
515 dissociated with Accutase (Thermo Fisher Scientific) and washed with D-PBS, followed by
516 resuspending the cells in 1x PBS without Mg^{2+}/Ca^{2+}, 0.5% FCS, 2.5 µM Rock Inhibitor and passed
517 through a 35 µm cell strainer (Corning). HEK293T and N2a cells co-transfected with pMAX-GFP were
518 sorted for the top 30% GFP-positive population. For the XMAS-TREE reporter assay in hiPSCs, only
519 cells co-expressing GFP and mCherry were sorted. FACS sorting was performed with either a
520 BD FACSAriaIII or BD FACSAria Fusion at the Flow Cytometry & FACS Core Facility (FFCF),
521 Zentrum für Molekulare Biologie der Universität Heidelberg (ZMBH) or FACS Core Facility (dFCCU),
522 Uniklinikum Heidelberg, respectively.

523 **Genomic DNA extraction from mammalian cell culture**

524 After FACS HEK293T, N2a cells were collected in 500 µl DMEM GlutaMAX supplemented with 10%
525 FBS. hiPSCs were collected in 500 µl StemMACS PSC-Brew XF medium supplemented with 2.5 µM
526 Rock Inhibitor. Cells were collected by centrifugation at 20,000 *x* g for 2 minutes, washed with 500 µl

527 D-PBS, and lysed in mammalian gDNA lysis buffer (10 mM Tris-HCl, 0.05% SDS, pH 8, 800 units
528 proteinase K (NEB)) for 2 hours at 37°C to extract genomic DNA. Afterwards, proteinase K was
529 inactivated for 30 min at 80°C. Cells transfected without fluorophore plasmid were washed once 72
530 hours after transfection, and then lysed in mammalian gDNA lysis buffer, as described above.

531 **Microinjection of mouse zygotes**

532 Injections were performed as previously described [79], with minor modifications. In brief, the injection
533 mix contained adenine base editor mRNA (100 ng/µl) and sgRNAs (50 ng/µl each; 12.5 ng/µl each, for
534 pooled sgRNA injections) in injection buffer (10 mM Tris-HCl, 0.25 mM EDTA, pH 7.4) to a final
535 volume of 50 µl with molecular biology-grade water. To prevent clogging of the cannula, the injection
536 mix was filtered shortly before microinjection using a Corning Costar Spin-X 0.22 µm centrifuge tube
537 filter. Zygotes were collected from timed matings and cultured *in vitro* in M2 medium during the
538 injection. Injection into the cytoplasm of zygote-stage embryos was conducted by carefully inserting
539 the injection needle at the equatorial level into the cytoplasm of each embryo, delivering a volume of
540 1-2 picolitres. Subsequently, the embryos were placed in preincubated M16 medium to select lysed and
541 intact embryos. Embryos were transferred on the same day via oviduct transfer to 0.5-day
542 pseudopregnant foster mothers.

543 **Genomic DNA extraction from mouse samples**

544 Embryonic day 14 mice were isolated from surrogate mothers. For DNA extraction, each embryo was
545 sectioned into smaller pieces, and genomic DNA was isolated using the DNeasy Blood & Tissue Kit
546 (Qiagen) following the manufacturer's protocol, with minor modifications. All reagents were applied
547 at double the recommended volume since the starting material exceeded 10 mg per embryo. Proteinase
548 K from New England Biolabs (NEB) was utilised instead of the kit-supplied enzyme.

549 For genotyping of founder mice, ear biopsies were obtained from the Interfakultäre Biomedizinische
550 Forschungseinrichtung of Heidelberg University. Genomic DNA was extracted from ear biopsy
551 samples using a lysis buffer consisting of DirectPCR Lysis Reagent (Mouse Tail) (Viagen Biotech) and
552 0.25 µg/µl Proteinase K (AppliChem). For lysis, each sample was incubated in 100-150 µl of this lysis
553 buffer at 55°C with vigorous shaking for a minimum of 4-5 hours, followed by inactivation of
554 Proteinase K at 85°C for 45 minutes. The lysate is subsequently used directly for PCR.

555 **Off-target analysis in mouse embryos**

556 The top five predicted off-target sites for each target locus were identified using ACEofBASEs [53] as
557 described under sgRNA design (**Supplementary Table 7-10**). ACEofBASEs provides links to
558 Ensembl gene IDs; therefore, the locus information for these sites was extracted from Ensembl.
559 Importantly, the column "distance" in the off-target list was used when exporting Ensembl sequence

560 information. In brief, when navigating the ENSEMBL genome browser, to export the locus information,
561 ensure the value of distance and an additional 1kb is added to the "5' Flanking sequence" and "3'
562 Flanking sequence". Primers were designed (Primer3 2.3.7) to flank the predicted off-target loci.

563 **Targeted deep sequencing and data analysis**

564 Samples were prepared for Amplicon-EZ-based NGS analysis (GeneWiz/Azenta Life Sciences) as
565 previously described [53]. All locus-specific primers contained the 5' partial Illumina adapter sequences
566 (Fwd: 5'-ACACTCTTTCCCTACACGACGCTCTTCCGATCT-3', Rev: 5'-
567 GACTGGAGTTCAGACGTGTGCTCTTCCGATCT-3'), and are listed in **Supplementary Table 5**.
568 Typically, samples corresponding to different target loci from each biological replicate were pooled
569 into a single sample. The pooled NGS data were demultiplexed by mapping to the respective reference
570 sequences later.

571 For a higher level of sample multiplexing, a sequencing library with indexing primers that include
572 unique i5 and i7 indexes, as well as P5 and P7 adapter sequences, was established. In brief, following
573 the preparation of PCR amplicons with locus-specific primers as described above (PCR1), a second
574 round of PCR was performed on these amplicons to barcode each sample, thereby allowing for the
575 pooling of samples from both the same and different target sites (PCR2). The primer pairs for the second
576 PCR contain complementary regions to the partial Illumina adapters along with the unique i5 and i7
577 index combinations (**Supplementary Table 6)**. For multiplexing, PCR1 samples were amplified using
578 Q5 Hot Start DNA polymerase (NEB) for 27 cycles, validated by agarose gel electrophoresis of a
579 subsample, and diluted between 1:5 and 1:20 based on gel band density. PCR2 was then set up at a
580 volume of 20 µl, containing 1 µl of the diluted PCR1 product, 0.5 µM of each forward (i5) and reverse
581 primer (i7) to create a combinatorial dual-index library, and Phusion U Green Multiplex PCR Master
582 Mix (Thermo Fisher Scientific); it was amplified for an additional 13 cycles. Individual PCR2
583 amplification was validated by agarose gel electrophoresis of a subsample, and 24 PCR2 samples were
584 pooled, run on a 1% agarose gel, with specific bands excised and cleaned up using the Monarch DNA
585 Gel Extraction Kit (NEB), measured by Qubit 4 Fluorometer (Thermo) using the Qubit dsDNA BR
586 Assay Kit, and pooled to equimolarity totalling 1 µg DNA. Samples were sequenced by GeneWiz
587 (Azenta Life Sciences) using the Sequencing only service with a 5% PhiX spike-in on an Illumina
588 MiSeq with 2 x 250 bp, paired-end sequencing, at a depth of approximately 10 million reads.

589 NGS data (in fastq.gz format) were processed and analysed using CRISPResso2 version 2.2.11 [80]. In
590 brief, two types of analyses were run in batch mode. First, all samples were analysed in base editing
591 mode with the following custom input parameters: --min_average_read_quality, 30; --
592 quantification_window_size, 20; --quantification_window_center, -10;
593 --base_editor_output. Downstream analysis was conducted using R version 4.2.1 in R Studio (packages:
594 tidyverse, ggplot, ggpubr, cowplot), with data used to plot Adenines across the protospacer sourced

from the "Nucleotide_percentage_summary_around_sgRNA.txt" output file. "Precision" (Supplementary Figure 1) was calculated as previously described [21] by dividing the second highest adenine-based editing frequency by the highest (A5 or A6); for this purpose, the indel frequency was extracted from the "CRISPRessoBatch_quantification_of_editing_frequency.txt" file and calculated as previously described [53].

Second, to quantify precise gene editing outcomes, the HDR mode was employed with the following custom input parameters: --min_average_read_quality, 30; --expected_hdr_amplicon_seq; --quantification_window_coordinates, "spacer-7nt (upstream)" – "spacer+PAM sequence (+3nt)"; --discard_indel_reads, TRUE. Downstream analysis was conducted using R, as described above, with data sourced from the "CRISPRessoBatch_quantification_of_editing_frequency.txt" file, with slight modifications following [81]. In short, for each sample's HDR amplicon, values under "Reads_aligned_all_amplicons", "Reads_aligned", "Unmodified", "Modified", and "Discarded" (HDR) were collected; additionally, the values under "Discarded" (REF) from the Reference amplicon were obtained. Specific values were then calculated as follows:

$$\text{Specified mutation, incl. bystander edits (\%)} = \frac{\text{“Reads_aligned”}}{\text{“Reads_aligned_all_amplicons”}} \times 100 \qquad (1)$$

$$\text{Specified mutation without bystander edits (\%)} = \frac{\text{“Unmodified”}}{\text{“Reads_aligned_all_amplicons”}} \times 100 \qquad (2)$$

$$\text{Purity (\%)} = \frac{\text{“Unmodified”}}{\text{“Reads_aligned”}} \times 100 \qquad (3)$$

$$\text{Indels (\%)} = \frac{\text{“Discarded” (HDR)+ “Discarded” (REF)}}{\text{“Reads_aligned_all_amplicons”}} \times 100 \qquad (4)$$

Statistics and graphics

All data reported in the text are presented as mean ± standard deviation (SD). Where appropriate (n≥20), we also reported the median (Q2) and interquartile range (IQR) between the first quartile (Q1) and the third quartile (Q3). Statistical comparisons were conducted using two-tailed Welch's *t*-test, as specified in the figure legends. Details on data reporting, including sample sizes and the statistical methods employed in each experiment, are provided in the figure legends. Data demonstrating statistical significance are depicted in the figures. Analysis and graphical data visualisation were performed in R version 4.2.1 with the Tidyverse, ggplot2, ggpubr, and cowplot packages [82-85]. Figures were assembled in Adobe Illustrator, with some icons and schemes imported from Biorender.

ACKNOWLEDGEMENTS

Sayari Bhunia is a member of HBIGS, the Heidelberg Biosciences International Graduate School. We thank the entire Freichel lab for their constructive feedback on the manuscript. We thank Maren Schneider for help with cloning pEF1α_ABE9-SpRY and XMAS-TREE sgRNAs. We thank the whole team from the Interfakultäre Biomedizinische Forschungseinrichtung (IBF) at Heidelberg University for their expert technical assistance. We thank Angela Wirth for writing the animal proposal. While preparing this work, the authors used AI-assisted technologies (Grammarly and ChatGPT) to improve readability and language.

AUTHOR CONTRIBUTIONS

Jun Kai Ong: Conceptualisation, Data curation, Formal analysis, Investigation, Methodology, Validation, Visualisation, Writing – original draft, Writing – review & editing. Sayari Bhunia: Investigation, Validation, Writing – review & editing. Beate Hilbert: Investigation. Vanessa Kirschner: Investigation, Writing – review & editing. Sascha Duglosz: Investigation. Frank Zimmermann: Investigation. Marc Freichel: Conceptualisation, Funding acquisition, Resources, Writing – review & editing. Alex Cornean: Conceptualisation, Data curation, Formal analysis, Methodology, Project administration, Supervision, Visualisation, Writing – original draft, Writing – review & editing.

SUPPLEMENTARY DATA

Supplementary Data will be made available online.

CONFLICT OF INTEREST

Alex Cornean is a co-founder and shareholder of DataHarmony Ltd, a company that provides gene editing-related services and software solutions.

FUNDING

This research was funded by the German Research foundation (DFG) through the Collaborative Research Centres CRC1550 (FKZ 464424253, projects B09 and S01), CRC1328 (335447717, project A21), DFG project FR 1638/5-1 (531047917), the DZHK (German Centre for Cardiovascular Research) and the BMBF (German Ministry of Education and Research); and The Health + Life Science Alliance Heidelberg Mannheim.

DATA AVAILABILITY

Oligonucleotide and sgRNA sequences used in this study are listed in Supplementary Tables 2, 3, 5, and 6. All raw NGS sequencing data generated in this study were in the NCBI Sequence Read Archive (SRA) database as a BioProject with the accession number PRJNA1291991. pCMV_ABE9-SpRY and

654 pEF1α_ABE9-SpRY will be made available through Addgene. Any other data and reagents will be
655 made available upon reasonable request.

656 **AUTHOR ORCIDS**

657 Jun Kai Ong: https://orcid.org/0009-0005-1865-9465

658 Marc Freichel: https://orcid.org/0000-0003-1387-2636

659 Alex Cornean: http://orcid.org/0000-0003-3727-7057

REFERENCES

1 Williams, R. W. in *Princ. Mol. Med.* (eds Marschall S. Runge & Cam Patterson) 53-60 (Humana Press, 2006).

2 Perlman, R. L. Mouse models of human disease: An evolutionary perspective. *Evol. med. public health* **2016**, 170-176 (2016). https://doi.org:10.1093/emph/eow014

3 Smith, P., DiLillo, D. J., Bournazos, S., Li, F. & Ravetch, J. V. Mouse model recapitulating human Fcγ receptor structural and functional diversity. *Proc. Natl. Acad. Sci. U.S.A.* **109**, 6181-6186 (2012). https://doi.org:doi:10.1073/pnas.1203954109

4 Scherrer, G. *et al.* Knockin mice expressing fluorescent δ-opioid receptors uncover G protein-coupled receptor dynamics *in vivo*. *Proc. Natl. Acad. Sci. U.S.A.* **103**, 9691-9696 (2006). https://doi.org:doi:10.1073/pnas.0603359103

5 Lee, H. Genetically Engineered Mouse Models for Drug Development and Preclinical Trials. *Biomol. Ther.* **22**, 267-274 (2014). https://doi.org:10.4062/biomolther.2014.074

6 Passier, R., Orlova, V. & Mummery, C. Complex Tissue and Disease Modeling using hiPSCs. *Cell Stem Cell* **18**, 309-321 (2016). https://doi.org:10.1016/j.stem.2016.02.011

7 Cong, L. *et al.* Multiplex genome engineering using CRISPR/Cas systems. *Science* **339**, 819-823 (2013). https://doi.org:10.1126/science.1231143

8 Takata, M. *et al.* Homologous recombination and non‐homologous end‐joining pathways of DNA double‐strand break repair have overlapping roles in the maintenance of chromosomal integrity in vertebrate cells. *EMBO J.* **17**, 5497-5508 (1998). https://doi.org:https://doi.org/10.1093/emboj/17.18.5497

9 Kosicki, M., Tomberg, K. & Bradley, A. Repair of double-strand breaks induced by CRISPR–Cas9 leads to large deletions and complex rearrangements. *Nat. Biotechnol.* **36**, 765-771 (2018). https://doi.org:10.1038/nbt.4192

10 Hwang, G.-H. *et al.* Large DNA deletions occur during DNA repair at 20-fold lower frequency for base editors and prime editors than for Cas9 nucleases. *Nat. Biomed. Eng.* **9**, 79-92 (2025). https://doi.org:10.1038/s41551-024-01277-5

11 Fiumara, M. *et al.* Genotoxic effects of base and prime editing in human hematopoietic stem cells. *Nat. Biotechnol.* **42**, 877-891 (2024). https://doi.org:10.1038/s41587-023-01915-4

12 Gaudelli, N. M. *et al.* Programmable base editing of A•T to G•C in genomic DNA without DNA cleavage. *Nature* **551**, 464-471 (2017). https://doi.org:10.1038/nature24644

13 Komor, A. C., Kim, Y. B., Packer, M. S., Zuris, J. A. & Liu, D. R. Programmable editing of a target base in genomic DNA without double-stranded DNA cleavage. *Nature* **533**, 420-424 (2016). https://doi.org:10.1038/nature17946

14 Rees, H. A. & Liu, D. R. Base editing: precision chemistry on the genome and transcriptome of living cells. *Nat. Rev. Genet.* **19**, 770-788 (2018). https://doi.org:10.1038/s41576-018-0059-1

15 Gaudelli, N. M. *et al.* Directed evolution of adenine base editors with increased activity and therapeutic application. *Nat. Biotechnol.* **38**, 892-900 (2020). https://doi.org:10.1038/s41587-020-0491-6

16 Wu, X. *et al.* Genome-wide binding of the CRISPR endonuclease Cas9 in mammalian cells. *Nat. Biotechnol.* **32**, 670-676 (2014). https://doi.org:10.1038/nbt.2889

17 Hsu, P. D. *et al.* DNA targeting specificity of RNA-guided Cas9 nucleases. *Nat. Biotechnol.* **31**, 827-832 (2013). https://doi.org:10.1038/nbt.2647

18 Grünewald, J. *et al.* Transcriptome-wide off-target RNA editing induced by CRISPR-guided DNA base editors. *Nature* **569**, 433-437 (2019). https://doi.org:10.1038/s41586-019-1161-z

19 Li, S., Liu, L., Sun, W., Zhou, X. & Zhou, H. A large-scale genome and transcriptome sequencing analysis reveals the mutation landscapes induced by high-activity adenine base editors in plants. *Genome Biol.* **23**, 51 (2022). https://doi.org:10.1186/s13059-022-02618-w

20 Richter, M. F. *et al.* Phage-assisted evolution of an adenine base editor with improved Cas domain compatibility and activity. *Nat. Biotechnol.* **38**, 883-891 (2020). https://doi.org:10.1038/s41587-020-0453-z

21 Chen, L. *et al.* Engineering a precise adenine base editor with minimal bystander editing. *Nat. Chem. Biol.* **19**, 101-110 (2023). https://doi.org:10.1038/s41589-022-01163-8

22 Walton, R. T., Christie, K. A., Whittaker, M. N. & Kleinstiver, B. P. Unconstrained genome targeting with near-PAMless engineered CRISPR-Cas9 variants. *Science* **368**, 290-296 (2020). https://doi.org:doi:10.1126/science.aba8853

23 Liao, J. *et al.* Therapeutic adenine base editing of human hematopoietic stem cells. *Nat. Commun.* **14**, 207 (2023). https://doi.org:10.1038/s41467-022-35508-7

24 Patel, S. & Kilpatrick, B. S. Two-pore channels and disease. *Biochimica et Biophysica Acta (BBA) - Molecular Cell Research* **1865**, 1678-1686 (2018). https://doi.org:https://doi.org/10.1016/j.bbamcr.2018.05.004

25 García-Rúa, V. *et al.* Increased Expression of Fatty-Acid and Calcium Metabolism Genes in Failing Human Heart. *PLoS One* **7**, e37505 (2012). https://doi.org:10.1371/journal.pone.0037505

26 Deutsch, R., Kudrina, V., Freichel, M. & Grimm, C. Two-pore channel regulators - Who is in control? *Frontiers in Physiology* **Volume 15 - 2024** (2025). https://doi.org:10.3389/fphys.2024.1534071

27 Medert, R. *et al.* Genetic background influences expression and function of the cation channel TRPM4 in the mouse heart. *Basic Res. Cardiol.* **115**, 70 (2020). https://doi.org:10.1007/s00395-020-00831-x

28 Stallmeyer, B. *et al.* Mutational spectrum in the Ca2+-activated cation channel gene TRPM4 in patients with cardiac conductance disturbances. *Hum. Mutat.* **33**, 109-117 (2012). https://doi.org:https://doi.org/10.1002/humu.21599

29 Tu, T. *et al.* A precise and efficient adenine base editor. *Mol. Ther.* **30**, 2933-2941 (2022). https://doi.org:10.1016/j.ymthe.2022.07.010

30 Jeong, Y. K. *et al.* Adenine base editor engineering reduces editing of bystander cytosines. *Nat. Biotechnol.* **39**, 1426-1433 (2021). https://doi.org:10.1038/s41587-021-00943-2

31 Cao, X. *et al.* Engineering of near-PAMless adenine base editor with enhanced editing activity and reduced off-target. *Mol. Ther.--Nucleic Acids* **28**, 732-742 (2022). https://doi.org:https://doi.org/10.1016/j.omtn.2022.04.032

32 Zhang, Z. *et al.* Engineering an adenine base editor in human embryonic stem cells with minimal DNA and RNA off-target activities. *Mol. Ther.--Nucleic Acids* **29**, 502-510 (2022). https://doi.org:10.1016/j.omtn.2022.07.026

33 Li, G. *et al.* A novel base editor SpRY-ABE8e^{F148A} mediates efficient A-to-G base editing with a reduced off-target effect. *Mol. Ther.--Nucleic Acids* **31**, 78-87 (2023). https://doi.org:10.1016/j.omtn.2022.12.001

34 Xiong, X. *et al.* Split complementation of base editors to minimize off-target edits. *Nat. Plants* **9**, 1832-1847 (2023). https://doi.org:10.1038/s41477-023-01540-8

35 Zeng, H. *et al.* A split and inducible adenine base editor for precise in vivo base editing. *Nat. Commun.* **14**, 5573 (2023). https://doi.org:10.1038/s41467-023-41331-5

36 Kim, Y.-h. *et al.* Sniper2L is a high-fidelity Cas9 variant with high activity. *Nat. Chem. Biol.* **19**, 972-980 (2023). https://doi.org:10.1038/s41589-023-01279-5

37 Wang, Z. *et al.* Decreasing predictable DNA off-target effects and narrowing editing windows of adenine base editors by fusing human Rad18 protein variant. *International Journal of Biological Macromolecules* **253**, 127418 (2023). https://doi.org:https://doi.org/10.1016/j.ijbiomac.2023.127418

38 Hu, J. H. *et al.* Evolved Cas9 variants with broad PAM compatibility and high DNA specificity. *Nature* **556**, 57-63 (2018). https://doi.org:10.1038/nature26155

39 Kleinstiver, B. P. *et al.* Engineered CRISPR-Cas9 nucleases with altered PAM specificities. *Nature* **523**, 481-485 (2015). https://doi.org:10.1038/nature14592

40 Huang, T. P. *et al.* Circularly permuted and PAM-modified Cas9 variants broaden the targeting scope of base editors. *Nat. Biotechnol.* **37**, 626-631 (2019). https://doi.org:10.1038/s41587-019-0134-y

41 Nishimasu, H. *et al.* Engineered CRISPR-Cas9 nuclease with expanded targeting space. *Science* **361**, 1259-1262 (2018). https://doi.org:doi:10.1126/science.aas9129

42 Ran, F. A. *et al.* In vivo genome editing using Staphylococcus aureus Cas9. *Nature* **520**, 186-191 (2015). https://doi.org:10.1038/nature14299

43 Miller, S. M. *et al.* Continuous evolution of SpCas9 variants compatible with non-G PAMs. *Nat. Biotechnol.* **38**, 471-481 (2020). https://doi.org:10.1038/s41587-020-0412-8

44 Zhao, L. *et al.* PAM-flexible genome editing with an engineered chimeric Cas9. *Nat. Commun.* **14**, 6175 (2023). https://doi.org:10.1038/s41467-023-41829-y

45 Li, J. *et al.* Genome editing mediated by SpCas9 variants with broad non-canonical PAM compatibility in plants. *Molecular Plant* **14**, 352-360 (2021). https://doi.org:10.1016/j.molp.2020.12.017

46 Villiger, L. *et al.* In vivo cytidine base editing of hepatocytes without detectable off-target mutations in RNA and DNA. *Nat. Biomed. Eng.* **5**, 179-189 (2021). https://doi.org:10.1038/s41551-020-00671-z

47 Liu, Z. *et al.* Efficient generation of mouse models of human diseases via ABE- and BE-mediated base editing. *Nat. Commun.* **9**, 2338 (2018). https://doi.org:10.1038/s41467-018-04768-7

48 Ryu, S.-M. *et al.* Adenine base editing in mouse embryos and an adult mouse model of Duchenne muscular dystrophy. *Nat. Biotechnol.* **36**, 536-539 (2018). https://doi.org:10.1038/nbt.4148

49 Yang, L. *et al.* Increasing targeting scope of adenosine base editors in mouse and rat embryos through fusion of TadA deaminase with Cas9 variants. *Protein Cell* **9**, 814-819 (2018). https://doi.org:10.1007/s13238-018-0568-x

50 Fu, J. *et al.* Human cell based directed evolution of adenine base editors with improved efficiency. *Nat. Commun.* **12**, 5897 (2021). https://doi.org:10.1038/s41467-021-26211-0

51 Qian, Y. *et al.* A new compact adenine base editor generated through deletion of HNH and REC2 domain of SpCas9. *BMC Biol.* **21**, 155 (2023). https://doi.org:10.1186/s12915-023-01644-9

52 Zhao, D. *et al.* Engineered domain-inlaid Nme2Cas9 adenine base editors with increased on-target DNA editing and targeting scope. *BMC Biol.* **21**, 250 (2023). https://doi.org:10.1186/s12915-023-01754-4

53 Cornean, A. *et al.* Precise in vivo functional analysis of DNA variants with base editing using ACEofBASEs target prediction. *eLife* **11**, e72124 (2022). https://doi.org:10.7554/eLife.72124

54 Doman, J. L., Raguram, A., Newby, G. A. & Liu, D. R. Evaluation and minimization of Cas9-independent off-target DNA editing by cytosine base editors. *Nat. Biotechnol.* **38**, 620-628 (2020). https://doi.org:10.1038/s41587-020-0414-6

55 Joshi, J., Albers, C., Smole, N., Guo, S. & Smith, S. A. Human induced pluripotent stem cell-derived cardiomyocytes (iPSC-CMs) for modeling cardiac arrhythmias: strengths, challenges and potential solutions. *Frontiers in Physiology* **Volume 15 - 2024** (2024). https://doi.org:10.3389/fphys.2024.1475152

56 Cerneckis, J., Cai, H. & Shi, Y. Induced pluripotent stem cells (iPSCs): molecular mechanisms of induction and applications. *Signal Transduction and Targeted Therapy* **9**, 112 (2024). https://doi.org:10.1038/s41392-024-01809-0

57 Brookhouser, N. *et al.* A Cas9-mediated adenosine transient reporter enables enrichment of ABE-targeted cells. *BMC Biol.* **18**, 193 (2020). https://doi.org:10.1186/s12915-020-00929-7

58 Rosello, M. *et al.* Disease modeling by efficient genome editing using a near PAM-less base editor in vivo. *Nat. Commun.* **13**, 3435 (2022). https://doi.org:10.1038/s41467-022-31172-z

59 Zuo, E. *et al.* Cytosine base editor generates substantial off-target single-nucleotide variants in mouse embryos. *Science* **364**, 289-292 (2019). https://doi.org:doi:10.1126/science.aav9973

60 Lee, S.-H. *et al.* Bystander editing by adenine base editors impairs vision restoration in a mouse model of Leber congenital amaurosis. *Molecular Therapy Methods & Clinical Development* **33** (2025). https://doi.org:10.1016/j.omtm.2025.101461

61 Tuladhar, R. *et al.* CRISPR-Cas9-based mutagenesis frequently provokes on-target mRNA misregulation. *Nat. Commun.* **10**, 4056 (2019). https://doi.org:10.1038/s41467-019-12028-5

62 Höijer, I. *et al.* CRISPR-Cas9 induces large structural variants at on-target and off-target sites in vivo that segregate across generations. *Nat. Commun.* **13**, 627 (2022). https://doi.org:10.1038/s41467-022-28244-5

63 Liao, J. *et al.* Sequential Amino Acid Mutagenesis-Driven De Novo Evolution of Adenine Deaminases Enables Efficient In Vivo Base Editing in Primate. *bioRxiv*, 2025.2005.2014.653640 (2025). https://doi.org:10.1101/2025.05.14.653640

64 Xiao, Y.-L., Wu, Y. & Tang, W. An adenine base editor variant expands context compatibility. *Nat. Biotechnol.* **42**, 1442-1453 (2024). https://doi.org:10.1038/s41587-023-01994-3

65 Qin, W. *et al.* ABE-ultramax for high-efficiency biallelic adenine base editing in zebrafish. *Nat. Commun.* **15**, 5613 (2024). https://doi.org:10.1038/s41467-024-49943-1

66 Perrotta, R. M. *et al.* Machine Learning and Directed Evolution of Base Editing Enzymes. *bioRxiv*, 2024.2005.2017.594556 (2024). https://doi.org:10.1101/2024.05.17.594556

67 Zhao, N. *et al.* Evolved cytidine and adenine base editors with high precision and minimized off-target activity by a continuous directed evolution system in mammalian cells. *Nat. Commun.* **15**, 8140 (2024). https://doi.org:10.1038/s41467-024-52483-3

68 Chen, Q. *et al.* Engineering of Peptide-Inserted Base Editors with Enhanced Accuracy and Security. *Small* **21**, 2411583 (2025). https://doi.org:https://doi.org/10.1002/smll.202411583

69 Silverstein, R. A. *et al.* Custom CRISPR–Cas9 PAM variants via scalable engineering and machine learning. *Nature* (2025). https://doi.org:10.1038/s41586-025-09021-y

70 Peña-Gutiérrez, I., Olalla-Sastre, B., Río, P. & Rodríguez-Madoz, J. R. Beyond precision: evaluation of off-target clustered regularly interspaced short palindromic repeats/Cas9–mediated genome editing. *Cytotherapy* **27**, 279-286 (2025). https://doi.org:10.1016/j.jcyt.2024.10.010

71 Shi, Y., Inoue, H., Wu, J. C. & Yamanaka, S. Induced pluripotent stem cell technology: a decade of progress. *Nature Reviews Drug Discovery* **16**, 115-130 (2017). https://doi.org:10.1038/nrd.2016.245

72 Liu, C., Oikonomopoulos, A., Sayed, N. & Wu, J. C. Modeling human diseases with induced pluripotent stem cells: from 2D to 3D and beyond. *Development* **145** (2018). https://doi.org:10.1242/dev.156166

73 Heinzelmann, E. *et al.* iPSC-derived and Patient-Derived Organoids: Applications and challenges in scalability and reproducibility as pre-clinical models. *Current Research in Toxicology* **7**, 100197 (2024). https://doi.org:https://doi.org/10.1016/j.crtox.2024.100197

74 Chang, Y., Lan, F., Zhang, Y. & Ma, S. Crispr-Based Editing of Human Pluripotent Stem Cells for Disease Modeling. *Stem Cell Reviews and Reports* **20**, 1151-1161 (2024). https://doi.org:10.1007/s12015-024-10713-7

75 Nami, F. *et al.* Fast and Efficient Generation of Isogenic Induced Pluripotent Stem Cell Lines Using Adenine Base Editing. *The CRISPR Journal* **4**, 502-518 (2021). https://doi.org:10.1089/crispr.2021.0006

76 Anzalone, A. V. *et al.* Search-and-replace genome editing without double-strand breaks or donor DNA. *Nature* **576**, 149-157 (2019). https://doi.org:10.1038/s41586-019-1711-4

77 Alves, C. R. R. *et al.* Optimization of base editors for the functional correction of SMN2 as a treatment for spinal muscular atrophy. *Nat. Biomed. Eng.* **8**, 118-131 (2024). https://doi.org:10.1038/s41551-023-01132-z

78 Chen, P. J. *et al.* Enhanced prime editing systems by manipulating cellular determinants of editing outcomes. *Cell* **184**, 5635-5652.e5629 (2021). https://doi.org:10.1016/j.cell.2021.09.018

79 Medert, R. *et al.* Efficient single copy integration via homology-directed repair (scHDR) by 5′ modification of large DNA donor fragments in mice. *Nucleic Acids Res.* **51**, e14-e14 (2022). https://doi.org:10.1093/nar/gkac1150

80 Clement, K. *et al.* CRISPResso2 provides accurate and rapid genome editing sequence analysis. *Nat. Biotechnol.* **37**, 224-226 (2019). https://doi.org:10.1038/s41587-019-0032-3

81 Doman, J. L., Sousa, A. A., Randolph, P. B., Chen, P. J. & Liu, D. R. Designing and executing prime editing experiments in mammalian cells. *Nature Protocols* **17**, 2431-2468 (2022). https://doi.org:10.1038/s41596-022-00724-4

82 Wickham, H. *et al.* Welcome to the tidyverse. *J. Open Source Softw.* **4**, 1686 (2019). https://doi.org:10.21105/joss.01686

83 Wickham, H. ggplot2: Elegant Graphics for Data Analysis. *Springer-Verlag New York* (2016).

84 Kassambara, A. ggpubr: 'ggplot2' Based Publication Ready Plots. (2022).

85 Wilke, C. O. cowplot: Streamlined Plot Theme and Plot Annotations for 'ggplot2'. (2024).

TABLES AND FIGURES

FIGURES

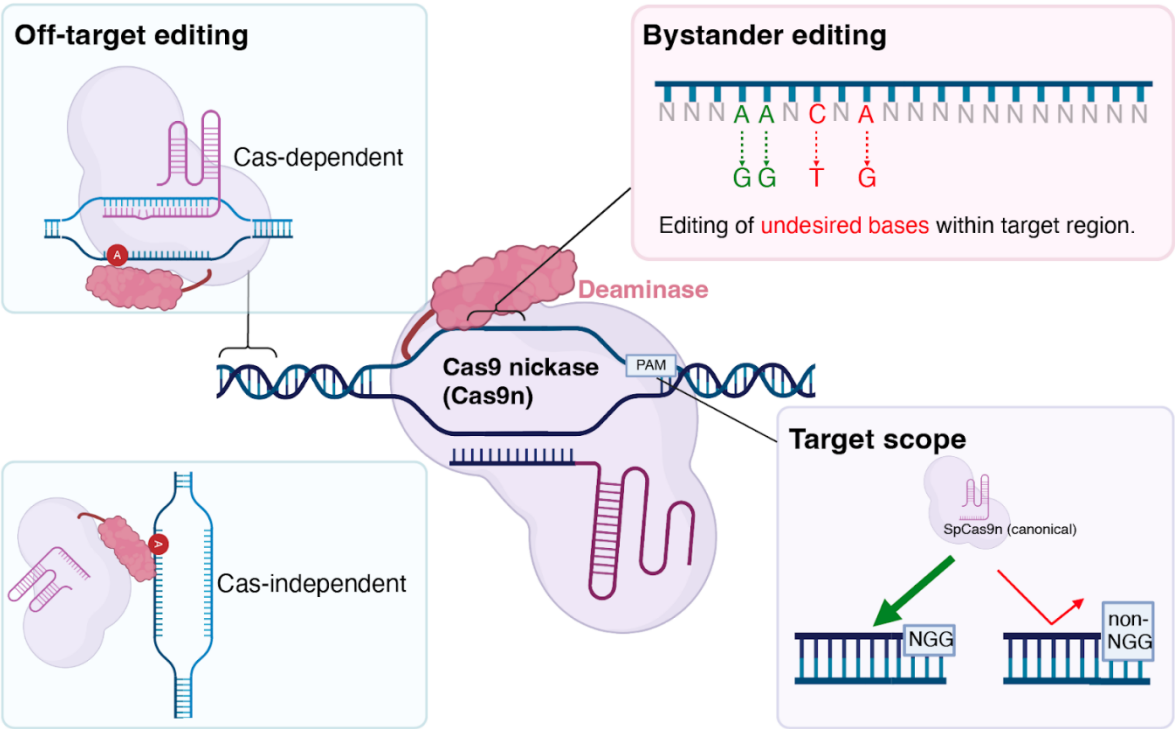

Figure 1 | Limitations of disease modelling with ABEs. Schematic of limitations of ABEs in generating disease models. ABEs can have Cas-dependent or -independent off-target editing. Besides targeted adenines, ABEs also have bystander activity on non-target bases. SpCas9 employed in ABEs recognises a 3' NGG PAM while does not bind optimally, or at all, to non-NGG PAM sites. This Figure was partially prepared with BioRender.

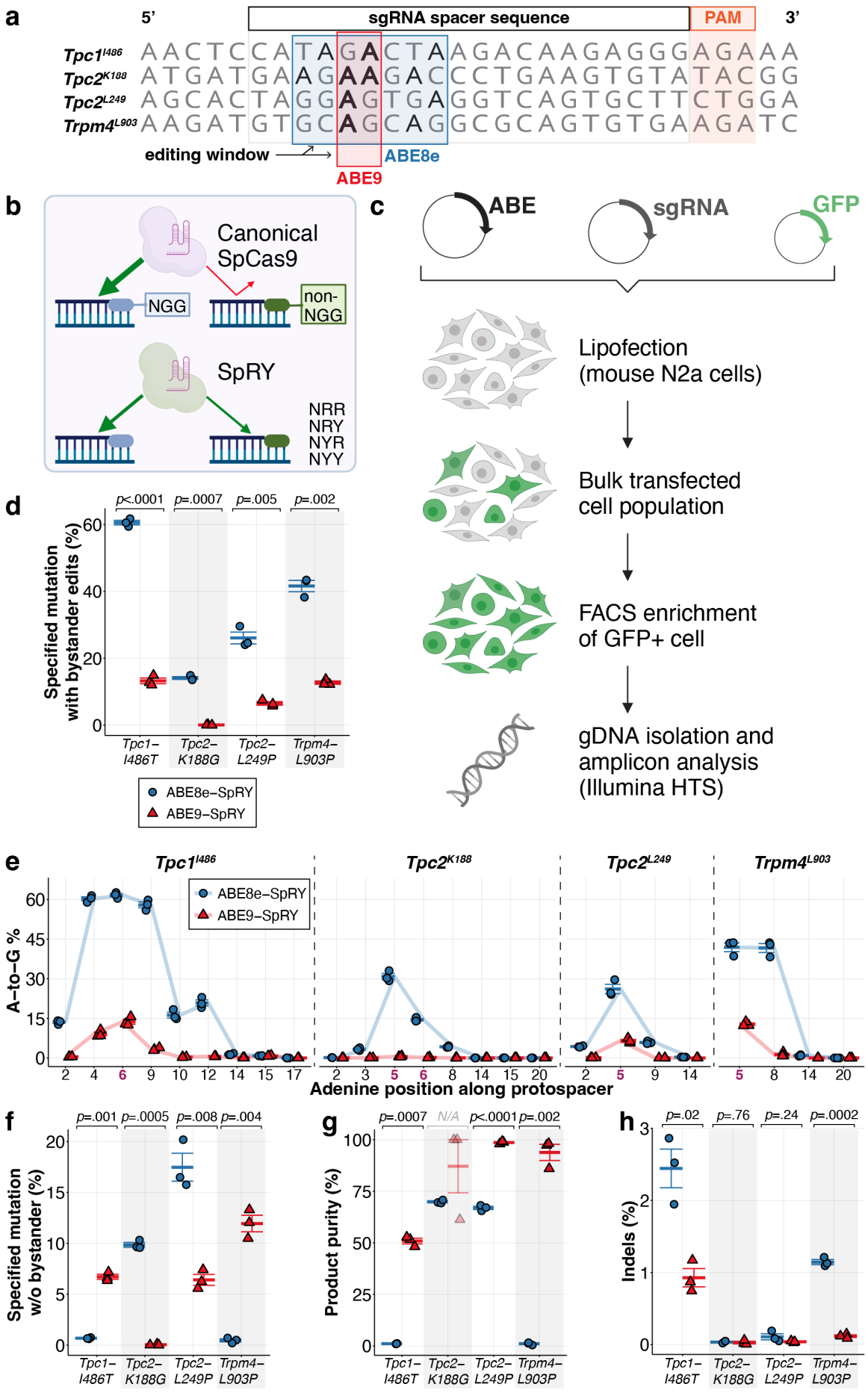
a
5'
sgRNA spacer sequence
PAM
3'
Tpc1I486 AACTCCATAGACTAAGACAAGAGGGAGAAA
Tpc2K188 ATGATGAAGAAGACCCTGAAGTGTATACGG
Tpc2L249 AGCACTAGGAGTGAGGTCAGTGCTTCTGGA
Trpm4L903 AAGATGTGCAGCAGGCGCAGTGTGAAGATC
editing window
ABE8e
ABE9
b
Canonical SpCas9
NGG
non-NGG
SpRY
NRR
NRY
NYR
NYY
c
ABE
sgRNA
GFP
Lipofection (mouse N2a cells)
Bulk transfected cell population
FACS enrichment of GFP+ cell
gDNA isolation and amplicon analysis (Illumina HTS)
d
Specified mutation with bystander edits (%)
p<.0001
p=.0007
p=.005
p=.002
Tpc1–I486T
Tpc2–K188G
Tpc2–L249P
Trpm4–L903P
ABE8e–SpRY
ABE9–SpRY
e
Tpc1I486
Tpc2K188
Tpc2L249
Trpm4L903
A–to–G %
ABE8e–SpRY
ABE9–SpRY
Adenine position along protospacer
f
Specified mutation w/o bystander (%)
p=.001
p=.0005
p=.008
p=.004
g
Product purity (%)
p=.0007
N/A
p<.0001
p=.002
h
Indels (%)
p=.02
p=.76
p=.24
p=.0002

Figure 2 | Evaluation of ABE-SpRY constructs in target sites of interest in mouse N2a cells. (**a**) Design of sgRNAs for optimal adenine base editing. Target adenines (bolded in red) for each locus are positioned within the optimal editing windows of ABE8e and ABE9 deaminases with the corresponding PAM sites shown. (**b**) The Cas9 variant SpRY can target non-NGG PAM sites, unlike the wild-type SpCas9. (**c**) N2a cells were co-transfected with three plasmids: the ABE plasmid, sgRNA plasmid, and GFP plasmid. GFP-positive cells were sorted, and genomic DNA (gDNA) was extracted for subsequent targeted sequencing analysis. (**d**) Maximum editing efficiency observed for the target adenine using ABE8e- or ABE9-SpRY, regardless of bystander editing. (**e**) A-to-G editing efficiencies of ABE8e and ABE9-SpRY at each adenine position along the protospacer region for the four target sites. The positions of adenines of interest are bolded in red. (**f**) Editing efficiency of the target adenine using ABE8e- or ABE9-SpRY, considering only reads without bystander editing or indels. (**g**) Product purity, calculated as the proportion of correctly edited sequences (F) relative to the total editing events (D), expressed as a percentage (F/D × 100%). (**h**) Frequency of indels at each of the four target sites. Data is presented as mean ± s.e.m., and individual data points are shown for three biological replicates. Parts of the schematics in (**c**) were created with BioRender.com.

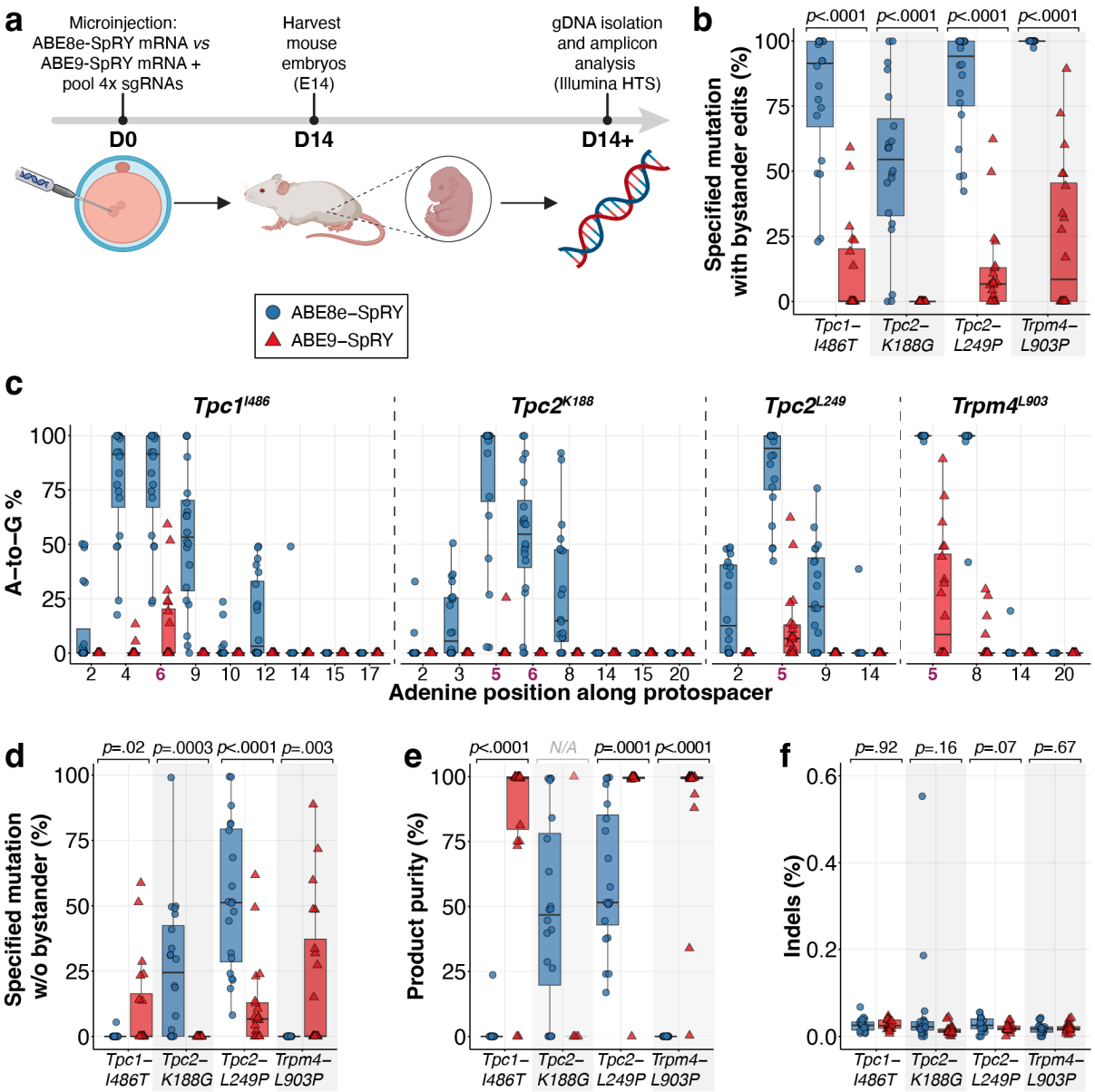

Figure 3 | Evaluation of ABE-SpRY constructs in target sites of interest in mouse embryos. (**a**) Schematic of generation of genetically edited mouse embryos. (**b**) Maximum editing efficiency observed for the target adenine, regardless of bystander editing. (**c**) A-to-G editing frequencies in twenty ABE8e or ABE9-SpRY edited mouse embryos at each adenine position along the protospacer region for the four target sites. Target adenines are bolded in red. (**d**) Maximum desired editing efficiency excluding cases with bystander editing. (**e**) Product purity, calculated as the proportion of correctly edited sequences (D) relative to the total editing events (B), expressed as a percentage (D/B × 100%). (**f**) Frequency of indel occurrence at the four target sites. Data are displayed as standard boxplots following the Tukey convention, including the median (horizontal line), and individual data points are shown for 20 independent biological replicates. Parts of the schematics in (**a**) were created with BioRender.com.

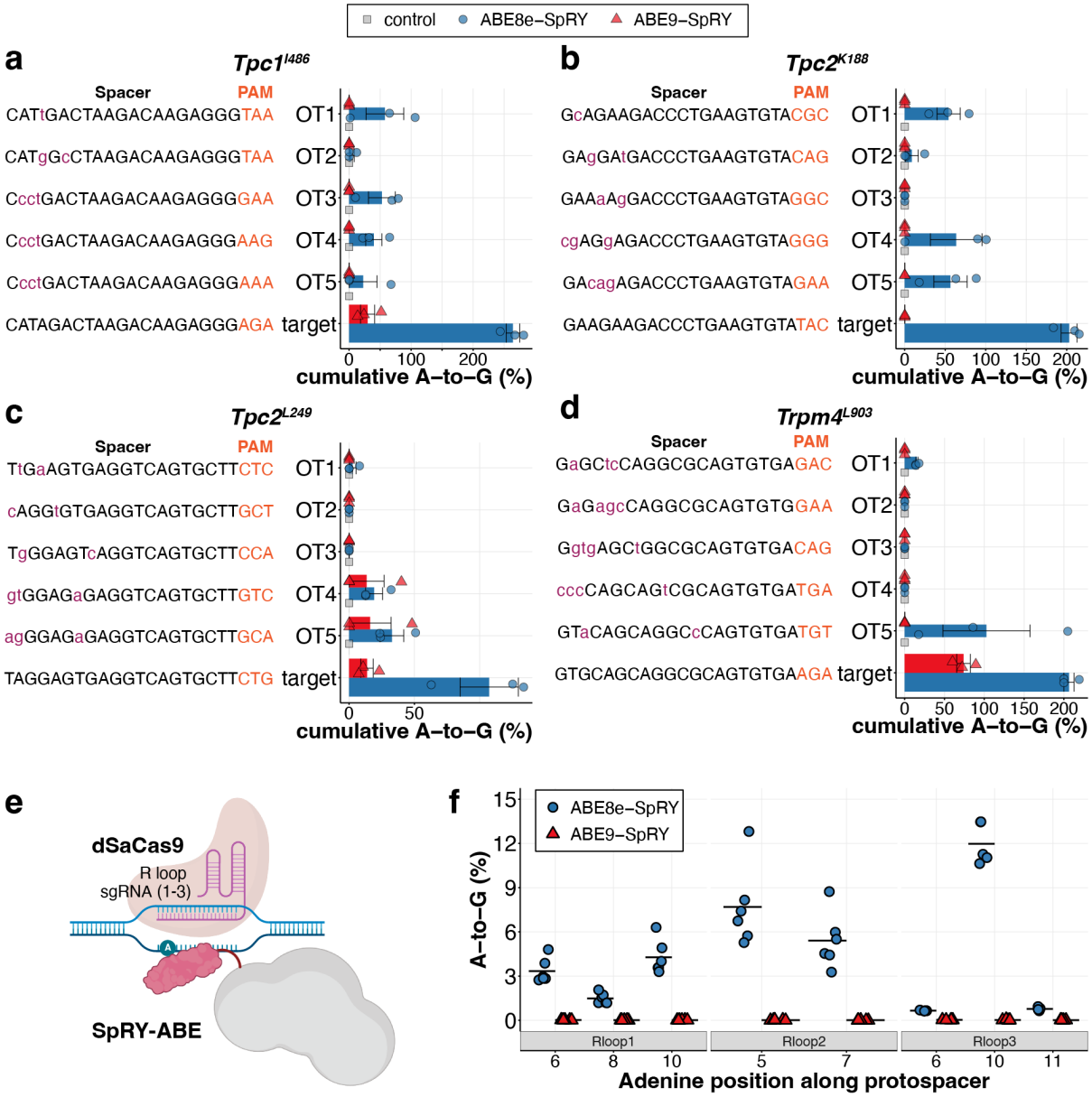

Figure 4 | Off-target mutation analysis of ABE-SpRY constructs. (**a-d**) Evaluation of cumulative on- and off-target DNA editing by ABE8e- and ABE9-SpRY in mouse embryos in a Cas9-dependent manner. Data represents mean ± s.e.m. from three biological replicates. (**e**) Diagram of the R-loop assay illustrating how the base editor can target transient non-target R-loops formed by dSaCas9. (**f**) Cas9-independent assessment of off-target DNA editing by ABE8e-SpRY and ABE9-SpRY, using the orthogonal R-loop assay at specific R-loop sites with five or six biological replicates. The black horizontal bar shows the mean at each adenine position grouped by editor. Parts of the schematics in (**e**) were created with BioRender.com.

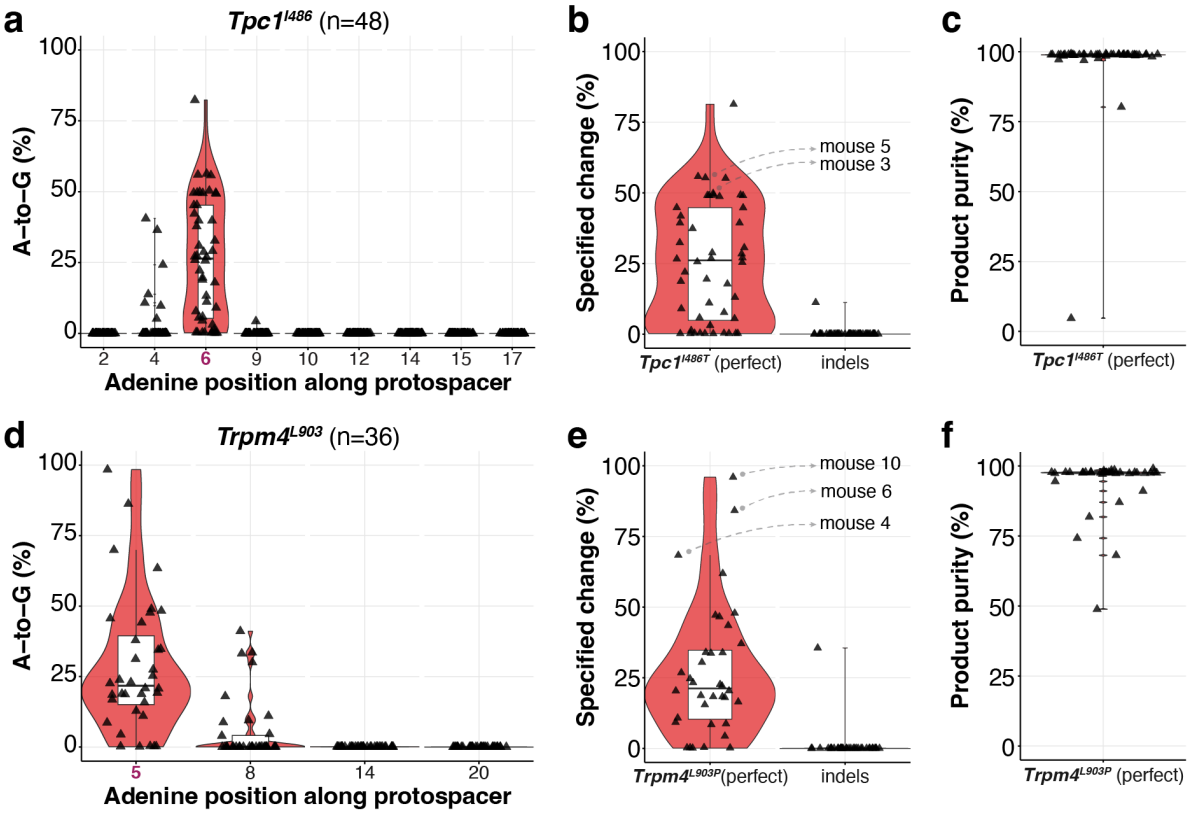

g

Tpc1 p.I486T

F0 ♂		F0 ♀
mouse 3	X	C57BL/6N
mouse 5	X	C57BL/6N

→

F1 id	n	+/+	+/-	%	F1 ♂		F1 ♀
m3-F1	8	3	5	62.5	m3-F1_6 (+/-)	X	C57BL/6N
m5-F1	9	4	5	55.6	m3-F1_7 (+/-)	X	C57BL/6N
					m5-F1_7 (+/-)	X	C57BL/6N

→

F2 id	n	+/+	+/-	%
m3_6-F2	9	6	3	33.3
m3_7-F2	6	3	3	50
m5_7-F2	7	6	1	14.3

h

Trpm4 p.L903P

F0 ♂		F0 ♀
mouse 4	X	C57BL/6N
mouse 6	X	C57BL/6N
mouse 10	X	C57BL/6N

→

F1 id	n	+/+	+/-	%	F1 ♂		F1 ♀
m4-F1	10	2	8	80	m4-F1_6 (+/-)	X	C57BL/6N
m6-F1	9	0	9	100	m6-F1_7 (+/-)	X	C57BL/6N
m10-F1	4	0	4	100			

→

F2 id	n	+/+	+/-	%
m4_6-F2	10	5	5	50
m6_7-F2	7	6	1	14.3

Figure 5 | ABE9-SpRY can effectively produce *Tpc1*^{I486T} and *Trpm4*^{L903P} founder mice. A-to-G editing frequencies plotted across each adenine position are shown in (**a**) for 48 *Tpc1*^{I486} adult mouse biopsies, and (**d**) for 36 *Trpm4*^{L903} adult mouse biopsies. The frequency of desired editing (without bystander edits) and indels are presented in (**b**) for *Tpc1*^{I486} adults, and (**e**) for *Trpm4*^{L903} adult mice. Product purity is calculated as the percentage of correctly edited sequences relative to the total number of modified alleles and is displayed in (**c**) for *Tpc1*^{I486} adults, and (**f**) for *Trpm4*^{L903} adult mice. Data are presented as standard boxplots (white) following the Tukey convention, which includes the median (black horizontal line), displayed within violin plots (red), and individual data points (black) representing each biological replicate. Crossing schemes of F0 founder mice, with numerical data for F1 and F2 transmission for *Tpc1*^{I486T} (**g**), and *Trpm4*^{L903P} (**h**), respectively.

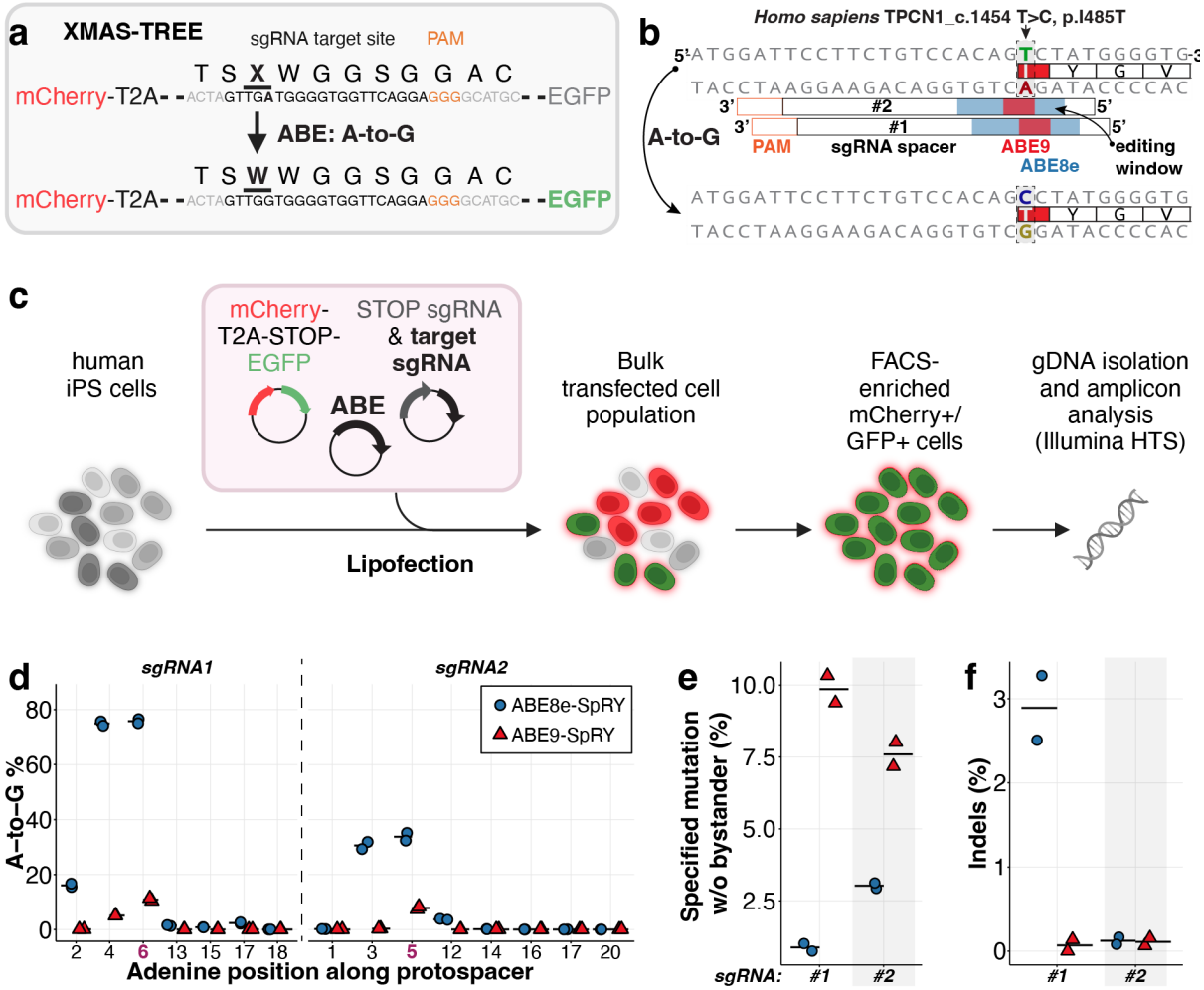

Figure 6 | Enrichment and analysis of base-edited hiPSC populations via XMAS-TREE. (**a**) Diagram of the X-MAS TREE system, illustrating the expression of an mCherry cassette followed by a stop codon (TGA) and a GFP cassette. Conversion of the adenine in the stop codon to guanine activates GFP expression. (**b**) Diagram showing the tiling of two sgRNAs across the target genomic region. (**c**) Schematic of the X-MAS TREE workflow for identifying and enriching adenine base-edited cells. Flow cytometry was used to isolate populations that are double-positive for mCherry and GFP for downstream sequencing. (**d**) Percentage of adenine-to-guanine conversions along the protospacer; (**e**) percentage of desired edits without bystander effects; and (**f**) percentage of indels observed with ABE8e-SpRY or ABE9-SpRY, using sgRNA1 or sgRNA2 in sorted cells. Horizontal bars represent the mean from two biological replicates. Parts of the schematics in **c** were created with BioRender.com.

Tables

Table 1. Overview of available approaches to overcome precision, off-target (OT) and targetability issues.

Goal	Type	Editor	Efficiency *	Editing window (vs 3-10*)	Off-targets*	Ref
Precision	Deaminase mutations	ABE9e-NG (R111T ,N127K, Q154R)	Similar	(3)4-7(8) at similar activity	**reduced DNA and RNA OTs**	29
		ABE8e-N108Q	Similar	4-7		
		ABE9 (N108Q, L145T)	**> -20%**	**5-6**		21
	Split editor	PIGS-ABE8e	> -40%	4-9	reduced DNA and RNA OTs	34
		sABE v3.22	> -25%	4-7		35
	Effector domain	ABE8e-e18	> -10%	5-7	reduced DNA OTs	37
Off-target reduction	Deaminase mutations	ABE8e-V106W	Similar	Similar	Reduction of DNA & RNA OTs	20
		ABE8.17-m-V106W	> -10%	Similar		15
		ABE8e-WA	Similar	4-8	Reduced RNA OTs	30
		ABE8e-WQ	> -20%	4-8		
	Deaminase mutation (+ Cas9 variant)	SpRY-ABE8e-F148A	Similar	Similar	Reduced RNA OTs	33
		CE-ABE8e-SpRY	Similar	Similar	Slightly reduced DNA OTs and reduced RNA OTs	31
		CE-ABE8e-dV-SpRY	Similar	Similar	Reduced indels, RNA and DNA OTs	32
	Cas9 variant	Sniper2L	Low mismatch tolerance (only 1 tolerated)			36
Target-ability	Cas9 variant	**ABEmax-SpRY**	**PAMless; targetability across NNN PAMs but likely massive increase in DNA OTs**			22
		ABE8e-SpRYc	PAMless; at certain selected loci more unbiased than ABE8e-SpRY			44

* mostly compared to ABE8e.